ANISOTROPIC MESH ADAPTATION FOR NUMERICAL SOLUTION OF BOUNDARY VALUE PROBLEMS [1]

Vít Dolejší and Jiří Felcman
Department of Numerical Mathematics
Faculty of Mathematics and Physics
Charles University
Sokolovská 83
186 00 Prague - Czech Republic

Abstract

We present an efficient mesh adaptation algorithm which can be successfully applied to numerical solutions of a wide range of 2D problems of physics and engineering described by partial differential equations. We are interested in the numerical solution of a general boundary value problem discretized on triangular grids. We formulate a necessary condition for properties of the triangulation on which the discretization error is below the prescribed tolerance and control this necessary condition by the interpolation error. For a sufficiently smooth function, we recall the strategy how to construct the mesh on which the interpolation error is below the prescribed tolerance. Solving the boundary value problem we apply this strategy to the smoothed approximate solution. The novelty of the method lies in the smoothing procedure that, followed by the anisotropic mesh adaptation (AMA) algorithm, leads to the significant improvement of numerical results. We apply AMA to the numerical solution of an elliptic equation where the exact solution is known and demonstrate practical aspects of the adaptation procedure: how to control the ratio between the longest and the shortest edge of the triangulation and how to control the transition of the coarsest part of the mesh to the finest one if the two length scales of all the triangles are clearly different. An example of the use of AMA for the physically relevant numerical simulation of a geometrically challenging industrial problem (inviscid transonic flow around NACA0012 profile) is presented.

1 Introduction

Numerical solutions of complicated problems of computational physics and mathematical engineering give rise to the necessity of application of adaptive methods which allow computation of a sufficiently precise solution without enormous requirements for memory and CPU time. The motivation of this paper were the works [21], [22] and [7]. The excellent review of the mesh generation research can be found in [25] and in the references therein. Our main results concern the smoothing of data produced by the numerical procedure in order to be able to apply the optimal interpolation error control meshing motivated by works cited. In [14] we developed the *anisotropic mesh adaptation* (AMA) algorithm which was applied to the computational fluid dynamics problems [12], [13]. The original approach of this algorithm was the use of the edge-based optimization criterion. This approach can be put in the frame of works [2] and [3]. Here we analyze more deeply the mathematical background of AMA

[1] This research has been supported under the Grant No. 275/2001/B–MAT/MFF of the Grant Agency of the Charles University Prague and the Grant No. MSM 113200007. The authors gratefully acknowledge this support.

and provide the reader with the algorithm for the application of AMA in the wide context of general numerical methods for solving a boundary value problem.

Let us consider a scalar boundary value problem (BVP) in the set Ω, where $\Omega \subset I\!R^2$ is a bounded domain. By $\overline{\Omega}$ and $\partial\Omega$ we denote the closure and boundary of Ω, respectively. We introduce the weak formulation of (BVP): Find the function $u : \Omega \to I\!R$ satisfying

$$u \in U, \tag{1}$$
$$\mathcal{L}(u, v) = f(v) \quad \forall v \in V, \tag{2}$$
$$\mathcal{B}(u) \in V. \tag{3}$$

Here U and V are the trial and test function spaces, respectively, (2) represents the weak form of the partial differential equation under consideration and (3) guarantees that the prescribed boundary conditions are fulfilled in the sense of traces. The function u satisfying (1) – (3) is called the *exact solution*. Let us suppose that the problem (1) – (3) has a unique exact solution.

Very often the numerical solution of (1) – (3) is sought in the space of piecewise polynomial functions and computed by a suitable numerical method (e.g. finite element method, finite volume method). To this end the domain Ω is replaced by its polygonal approximation Ω_h and the triangulation $\mathcal{T}_h$ is constructed. The *approximate solution* of problem (1) – (3) is defined as a function $u_h : \overline{\Omega}_h \to I\!R$ satisfying

$$u_h \in U_h, \tag{4}$$
$$\mathcal{L}_h(u_h, v_h) = f_h(v_h) \quad \forall v_h \in V_h, \tag{5}$$
$$\mathcal{B}_h(u_h) \in V_h. \tag{6}$$

Here

$$U_h = \left\{ u_h \in L^1(\Omega_h); u_h|_T \in P_k(T) \ \forall T \in \mathcal{T}_h \right\}, \tag{7}$$

$P_k(T) = \{p|_T; p \in P_k\}$, P_k denotes the set of all polynomials of degree $\leq k$ ($k \geq 0$) and $\mathcal{L}_h$, f_h, $\mathcal{B}_h$, V_h are the discrete analogues of $\mathcal{L}$, f, $\mathcal{B}$, V, respectively. Both possibilities $U_h \subset U$ and $U_h \not\subset U$ are admissible. Let us suppose that the *discrete problem* (4) – (6) has a unique solution u_h.

To measure how close the approximate solution u_h is to the exact solution u we define the *discretization error* as

$$e_h \equiv \|u - u_h\|_X, \tag{8}$$

where $\|\cdot\|_X$ is a suitable norm such that the expression $\|v\|_X$ has sense $\forall v \in U \cup U_h$. (If $U_h \subset U$ we can put $\|\cdot\|_X \equiv \|\cdot\|_U$, where $\|\cdot\|_U$ is the norm in the space U.)

The ultimate goal of the numerical method (4) - (6) for the solution of the problem (1) - (3) is to compute the approximate solution satisfying

$$e_h \leq \omega. \tag{9}$$

In what follows we present the necessary condition for the relation (9) and show on numerical examples how its satisfaction can be used for the construction of adaptive meshes.

We denote by $\mathcal{O}(U, U_h)$ the set of all operators from U to U_h, i.e.

$$\mathcal{O}(U, U_h) = \{\Pi, \Pi : w \in U \mapsto \Pi w \in U_h\}. \tag{10}$$

Let us consider the minimization problem: Find $\Pi_h \in \mathcal{O}(U, U_h)$ such that

$$\|w - \Pi_h w\|_X = \min_{w_h \in U_h} \|w - w_h\|_X \quad \forall w \in U. \tag{11}$$

The existence of Π_h follows from the fact that U_h is a finite dimensional space. The operator Π_h may not be uniquely determined, its uniqueness depends on the choice of $\|\cdot\|_X$.

It is evident that for the approximate solution u_h of (4) – (6)

$$\|u - \Pi_h u\|_X \leq e_h. \tag{12}$$

This is the crucial point of the proposed adaptation strategy: Any numerical method for the solution of (1) – (3) computes the approximate solution u_h with the discretization error which is bounded from below by $\|u - \Pi_h u\|_X$, where u is the exact solution of (1) – (3). Then the necessary condition to fulfill (9) is

$$\|u - \Pi_h u\|_X \leq \omega. \tag{13}$$

It is evident that the magnitude of $\|u - \Pi_h u\|_X$ strongly depends on the choice of U_h and therefore on the choice of $\mathcal{T}_h$. As the condition (13) is only necessary it says nothing else than if it is not satisfied then no numerical method for the solution of (4) - (6) can compute the approximate solution with the error satisfying (9). To give the numerical method (1) – (3) the chance to satisfy (9), the mesh on which (13) holds is needed.

For a given ω, the condition (13) is satisfied if the triangulation is sufficiently fine. This can be achieved

(i) by a global mesh refinement, which is rather inefficient from the point of view of computer memory and CPU time in further computations,

(ii) by a local grid refinement/coarsening/alignment strategy, which is the subject-matter of this paper.

The basic principle of AMA can be illustrated on the following 1D example. Let $\langle A, B\rangle \in \mathbb{R}^1$ be an interval with the partition $\mathcal{T}_h$ and $u \in C^2(\langle A, B\rangle)$ the function from Figure 1 (full line). Then for the function $\Pi_h u$ (dashed line) from the space $\{v_h \in L^1(\langle A, B\rangle); v_h|_T \in P_1(T)\ \forall T \in |T_h\}$ given by (11) where we set $\|\cdot\|_X = \|\cdot\|_{L^\infty(\langle A,B\rangle)}$, it holds that

$$\|u - \Pi_h u\|_X = \omega, \tag{14}$$

where $\max_{x\in\langle A,B\rangle} |u(x) - \Pi_h u(x)|$ is plotted in Figure 1, left.

Let $\omega_1 < \omega$, our aim is to construct the mesh $\mathcal{T}_{h_1}$ and to obtain

$$\|u - \Pi_{h_1} u\|_X \leq \omega_1. \tag{15}$$

AMA tries to achieve this goal without global refinement as it is shown in Figure 1, right. In this case the number of intervals of $\mathcal{T}_{h_1}$ is even smaller then for $\mathcal{T}_h$. If u from above is a solution of the problem (1) – (3) then $\mathcal{T}_{h_1}$ is a suitable mesh for the numerical solution of (4) – (6).

In practical problems, of course, the exact solution is not a priori known. In that case we compute the approximate solution u_h on the starting mesh $\mathcal{T}_h$, smooth u_h and apply the AMA algorithm to this smoothed function. The smoothing procedure is the key issue of this paper and it is demonstrated in Section 4.2.

We present practical results of the numerical simulation of transonic inviscid flow in Section 6 .

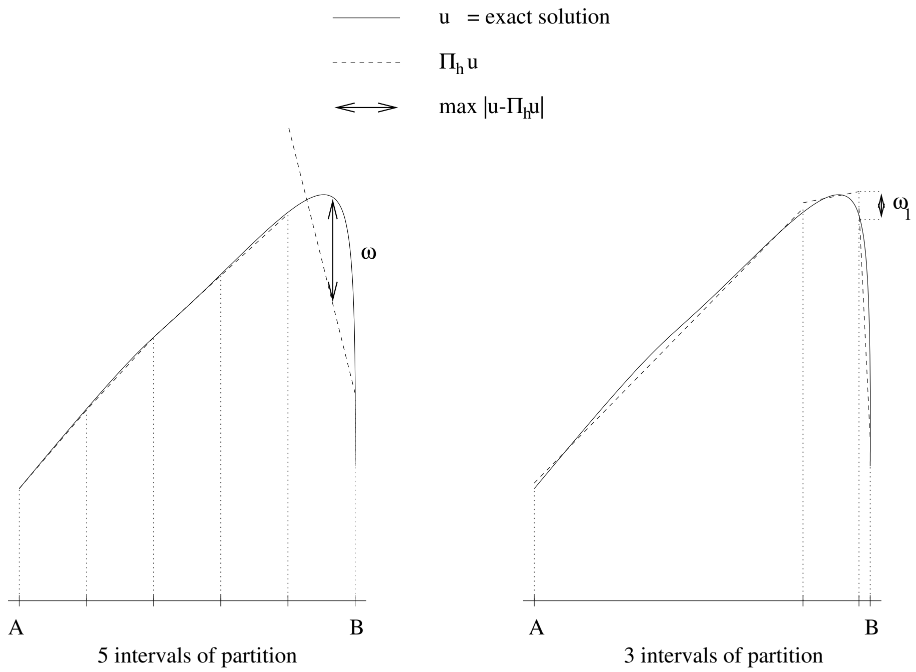

Figure 1: Motivation of AMA: partition of the interval AB, u is the exact solution, $\Pi_h u$ discontinuous piecewise linear function given by (14), $\max_{x\in(A,B)} |u - \Pi_h u|$ is denoted by $\leftrightarrow$.

2 Theoretical background of AMA

In the first part of this paper, for a given $\omega > 0$ and given function u we describe the construction of the triangulation $\mathcal{T}_h$ for which the function $\Pi_h u$ satisfies (13) and the triangulation has as small number of elements as possible. To do this explanation comprehensive we assume $u \in C^2(\bar{\Omega})$ with a positive definite Hesse matrix. This is a usual assumption, see, e.g., [25], where a quadratic data function is used. We do not impose any constraints on the change of second derivatives of u.

In the second part of the paper we apply these results to the non-smooth data function and present the numerical solution of a physically relevant problem.

From the practical point of view, we shall use piecewise linear polynomials in (7), i.e.

$$U_h = \left\{ u_h \in L^1(\Omega_h); u_h|_T \in P_1(T)\ \forall T \in \mathcal{T}_h \right\}, \tag{16}$$

and we set

$$\| \cdot \|_X = \| \cdot \|_{L^\infty(\Omega_h)}. \tag{17}$$

An example of function from U_h is viewed in Figure 2. This choice of U_h covers a wide range of numerical methods, piecewise constant approximation used in finite volume method (see, e.g., [17], [23], [24]) and conforming (see, e.g., [8]), nonconforming (see, e.g., [1], [15], [26]) and discontinuous finite element method (see, e.g., [9]). On the other hand the use of AMA does not require the piecewise linear approximation and a higher order approximation can be easily adopted for the efficient use of AMA.

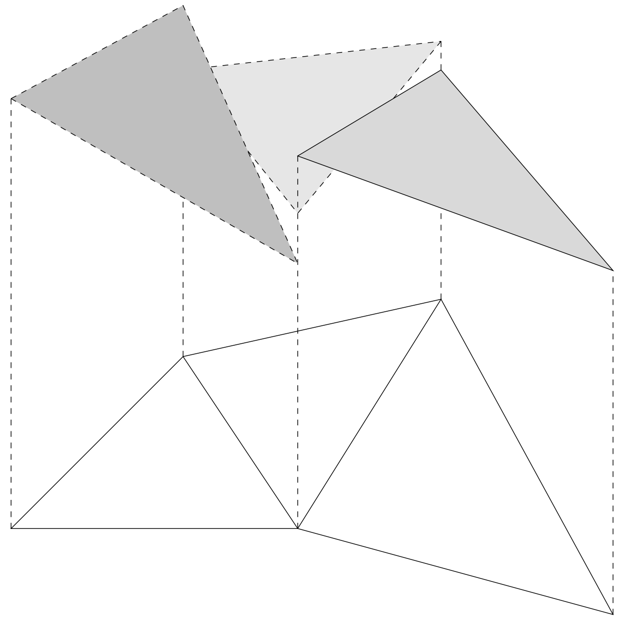

Figure 2: Example of linear discontinuous finite element.

2.1 ω-minimal triangulation

Definition 1 *Let $\Omega \subset I\!R^2$. We say that $\mathcal{T}_h = \{T_i\}_{i \in I}$ (I = an index set) is a* triangulation *of Ω if:*

1. *$T_i \in \mathcal{T}_h$ is a closed triangle.*
2. *$\bigcup_{i \in I} T_i = \overline{\Omega_h}$, where Ω_h is a polygonal approximation of Ω.*
3. *We denote by $\sigma_h = \{P_1, \ldots, P_N\}$ the set of all vertices of all $T \in \mathcal{T}_h$. We suppose that $\sigma_h \cap \partial\Omega_h \subset \partial\Omega$, $\sigma_h \subset \overline{\Omega}$.*
4. *For any $T_i, T_j \in \mathcal{T}_h$, $T_i \neq T_j$, $T_i \cap T_j$ are either disjoint or their intersection $T_i \cap T_j$ is a common vertex or $T_i \cap T_j$ is a common edge of T_i and T_j.*

The step size *h of the mesh is given by*

$$h = \max_{i \in I} diam(T_i), \tag{18}$$

where $diam(T_i)$ denotes the diameter of T_i.

Without proof we present the following lemma:

Lemma 1 *Let $\Omega \in I\!R^2$ be a computational domain and $\bar{h} > 0$. Then there exists a triangulation $\mathcal{T}_h$ of Ω with the step size h, $h \leq \bar{h}$.*

Definition 2 *Let $w \in C^2(\overline{\Omega})$ and $\mathcal{T}_h = \{T_i\}_{i \in I}$ be a triangulation of Ω. Let (x_i, y_i) be the center of gravity of $T_i \in \mathcal{T}_h$. We say that the operator $r_h \in \mathcal{O}(C^2(\overline{\Omega}), U_h)$ is the* ∇-interpolation *if*

$$\begin{aligned} r_h w(x_i, y_i) &= w(x_i, y_i) \qquad \forall T_i \in \mathcal{T}_h, (x_i, y_i) \in \Omega, \\ \nabla r_h w(x_i, y_i) &= \nabla w(x_i, y_i) \qquad \forall T_i \in \mathcal{T}_h, (x_i, y_i) \in \Omega. \end{aligned} \tag{19}$$

Lemma 2 *Let $w \in C^2(\overline{\Omega})$ and $\mathcal{T}_h = \{T_i\}_{i\in I}$ be a triangulation of Ω. Let U_h, $\|\cdot\|_X$, Π_h and r_h be given by (16), (17), (11) and (19), respectively. Then*

$$\|w - \Pi_h w\|_X \leq \|w - r_h w\|_X. \tag{20}$$

Proof. As $r_h w \in U_h$, the assertion follows immediately from (11). □

Remark 1 *Lemma 2 is valid also for more general $\|\cdot\|_X$.*

Definition 3 *Let u be the exact solution of the considered problem (1) – (3) in the computational domain Ω and r_h be the operator (19), where U_h is given by (16). The* interpolation error function $E_I : \Omega \cap \Omega_h \to I\!R^1$ *is defined by*

$$E_{\rm I}(x,y) = |u(x,y) - r_h u(x,y)| \text{ for almost every } (x,y) \in \Omega \cap \Omega_h. \tag{21}$$

Lemma 2 allows us to control the necessary condition (13) by the interpolation error function E_I, cf. [10], [11]. Therefore our aim is to construct a triangulation $\mathcal{T}_h$ of Ω so that the interpolation error function $E_{\rm I}(x,y)$ is bounded from above by a given tolerance. On the other hand, for computational reasons we need the number of elements of the triangulation to be as small as possible.

Let us stress that by the interpolation error function $E_{\rm I}(x,y)$ only the necessary condition (13) is controlled and not the discretization error (8).

Definition 4 *Let $u \in C^2(\overline{\Omega})$ and $\mathcal{T}_h = \{T_i\}_{i\in I}$ be a triangulation of Ω. Let $E_{\rm I}$ be given by (21). We say that $\mathcal{T}_h$ is an ω-*triangulation *if*

$$E_{\rm I}(x,y) \leq \omega \qquad \forall (x,y) \in \Omega \cap \Omega_h. \tag{22}$$

Theorem 1 *Let $u \in C^2(\overline{\Omega})$ and $\omega > 0$. Then there exists an ω-triangulation.*

Proof. For $u \in C^2(\overline{\Omega})$ there exists a constant $\hat{c} > 0$ such that

$$\left|\frac{\partial^2 u(x,y)}{\partial x^2}\right| \leq \hat{c}, \quad \left|\frac{\partial^2 u(x,y)}{\partial x \partial y}\right| \leq \hat{c}, \quad \left|\frac{\partial^2 u(x,y)}{\partial y^2}\right| \leq \hat{c}, \quad \forall (x,y) \in \overline{\Omega}. \tag{23}$$

Lemma 1 states that there exists a triangulation $\mathcal{T}_h$ with step size

$$h \leq \sqrt{\frac{\omega}{2\hat{c}}}. \tag{24}$$

We prove that $\mathcal{T}_h$ is an ω-triangulation. Let (x_i, y_i) be the center of gravity of $T_i \in \mathcal{T}_h$. There exists the uniquely defined function $r_h u$ given by (19). Then

$$r_h u(x,y) = u(x_i,y_i) + \frac{\partial u(x_i,y_i)}{\partial x}(x - x_i) + \frac{\partial u(x_i,y_i)}{\partial y}(y - y_i), \ (x,y) \in T_i. \tag{25}$$

Let $(x,y) \in \Omega \cap \Omega_h$, then there exists a triangle $T_i \in \mathcal{T}_h$ such that $(x,y) \in T_i$. Moreover, we suppose that $(x,y) + \vartheta(x_i - x, y_i - y) \in \overline{\Omega}\ \forall \vartheta \in \langle 0, 1\rangle$. Then the Taylor series expansion gives

$$\begin{aligned} u(x,y) &= r_h u(x_i,y_i) + \\ &+ \frac{1}{2}\left[\frac{\partial^2 u(\xi_x,\xi_y)}{\partial x^2}(x-x_i)^2 + 2\frac{\partial^2 u(\xi_x,\xi_y)}{\partial x \partial y}(x-x_i)(y-y_i) + \frac{\partial^2 u(\xi_x,\xi_y)}{\partial y^2}(y-y_i)^2\right], \end{aligned} \tag{26}$$

where (ξ_x, ξ_y) is a point lying between (x, y) and (x_i, y_i). As $|x - x_i| \leq h$ and $|y - y_i| \leq h$, then using (23) and (25), we have from (26)

$$|u(x,y) - r_h u(x,y)| \leq \frac{1}{2} 4\hat{c}h^2, \qquad x \in \Omega \cap \Omega_h, \tag{27}$$

which together with (24) proves the theorem. □

Definition 5 *Let $u \in C^2(\overline{\Omega})$. We say that $\mathcal{T}_h^{\min}$ is the* ω-minimal triangulation *if $\mathcal{T}_h^{\min}$ is an ω-triangulation and*

$$\mathrm{Card}(\mathcal{T}_\mathrm{h}^{\min}) = \min \mathrm{Card}(\mathcal{T}_\mathrm{h}), \tag{28}$$

where $\mathrm{Card}(\mathcal{T}_\mathrm{h})$ *denotes the number of elements of $\mathcal{T}_h$ and the minimum is taken over all ω-triangulations $\mathcal{T}_h$ of Ω.*

Theorem 2 *Let $u \in C^2(\overline{\Omega})$. Then there exists an ω-minimal triangulation.*

Proof. It follows from Theorem 1 that the set of ω-triangulations is not empty. As the function Card : $\mathcal{T}_h \to \mathbb{N}$ ($\mathbb{N}$ = natural numbers) is bounded from below it attains its minimum. □

2.2 Optimal triangle

In order to approach $\mathcal{T}_h^{\min}$ we introduce the concept of an *optimal triangle.* Let $u \in C^2(\overline{\Omega})$ and let its Hesse matrix $\boldsymbol{H}$

$$\boldsymbol{H}(x,y) = \begin{pmatrix} \frac{\partial^2 u}{\partial x^2} & \frac{\partial^2 u}{\partial x \partial y} \\ \frac{\partial^2 u}{\partial y \partial x} & \frac{\partial^2 u}{\partial y^2} \end{pmatrix} (x,y), \qquad (x,y) \in \Omega \tag{29}$$

be symmetric positive definite. Let $\mathcal{T}_h$ be an ω-triangulation and $r_h u$ be the ∇-interpolation given by (19). Let (x_i, y_i) be the center of gravity of $T_i \in \mathcal{T}_h$ and $(x, y) \in T_i \cap \Omega$. Then, using the Taylor series expansion at (x_i, y_i), we have

$$\begin{aligned} & u(x,y) = r_h u(x_i, y_i) + \\ + \quad & \frac{1}{2}\left[\frac{\partial^2 u(x_i,y_i)}{\partial x^2}(x-x_i)^2 + 2\frac{\partial^2 u(x_i,y_i)}{\partial x \partial y}(x-x_i)(y-y_i) + \frac{\partial^2 u(x_i,y_i)}{\partial y^2}(y-y_i)^2\right] + \\ + \quad & o(|x-x_i|^2 + |y-y_i|^2). \end{aligned}$$

In what follows we shall neglect the terms of order $o(|x - x_i|^2 + |y - y_i|^2)$ in equalities and inequalities. Up to terms of this order we can write

$$\begin{aligned} E_\mathrm{I}(x,y) &= |u(x,y) - r_h u(x,y)| = \\ &= \frac{1}{2}\left|\frac{\partial^2 u(x_i,y_i)}{\partial x^2}(x-x_i)^2 + 2\frac{\partial^2 u(x_i,y_i)}{\partial x \partial y}(x-x_i)(y-y_i) + \frac{\partial^2 u(x_i,y_i)}{\partial y^2}(y-y_i)^2\right|, \\ & \quad (x,y) \in T_i \cap \Omega. \end{aligned} \tag{30}$$

As $\mathcal{T}_h$ is the ω-triangulation we have

$$\begin{aligned} & \left|\frac{\partial^2 u(x_i,y_i)}{\partial x^2}(x-x_i)^2 + 2\frac{\partial^2 u(x_i,y_i)}{\partial x \partial y}(x-x_i)(y-y_i) + \frac{\partial^2 u(x_i,y_i)}{\partial y^2}(y-y_i)^2\right| \leq 2\omega, \\ & (x,y) \in T_i \cap \Omega, \end{aligned} \tag{31}$$

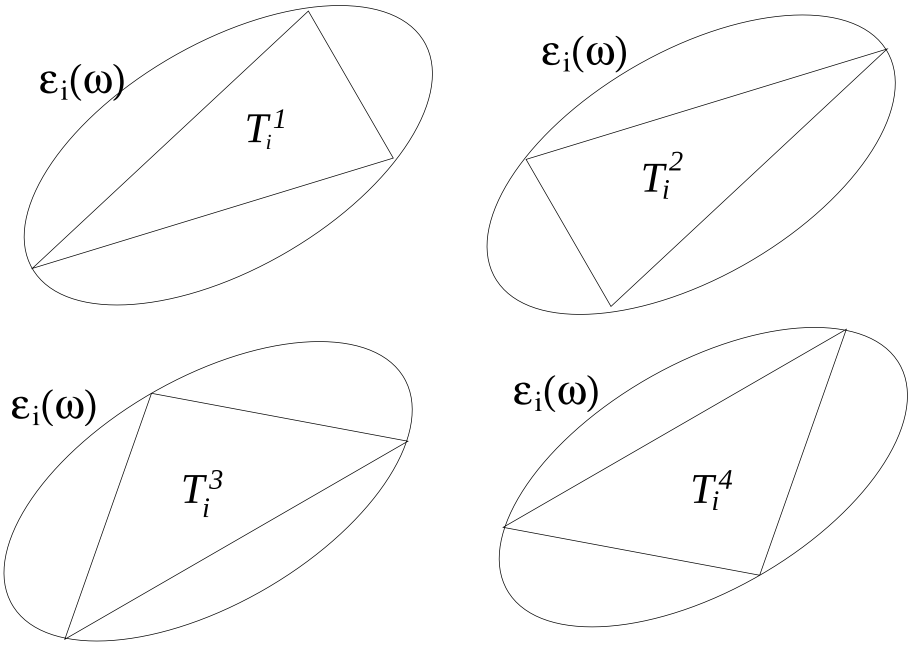

Figure 3: Ellipse $\varepsilon_i(\Omega)$ and the corresponding optimal triangles $T_i^1, \ldots, T_i^4$.

which can be rewritten as

$$\left(\begin{array}{cc} x - x_i, & y - y_i \end{array} \right) \left(\begin{array}{cc} \frac{\partial^2 u}{\partial x^2} & \frac{\partial^2 u}{\partial x \partial y} \\ \frac{\partial^2 u}{\partial x \partial y} & \frac{\partial^2 u}{\partial y^2} \end{array} \right)\Bigg|_{(x_i, y_i)} \left(\begin{array}{c} x - x_i \\ y - y_i \end{array} \right) \leq 2\omega, \ (x, y) \in T_i \cap \Omega. \tag{32}$$

The points $(x, y) \in I\!\!R^2$ satisfying the relation (32) form an ellipse $\varepsilon_i(\omega) \subset I\!\!R^2$, see [14]. From this it follows that the interpolation error function $E_{\mathrm{I}}(x, y)$ is bounded from above by ω for all $(x, y) \in \varepsilon_i(\omega)$. Consequently, if T is such a triangle that $T \subset \varepsilon_i(\omega)$ then $E_{\mathrm{I}}(x, y) \leq \omega$ for all $(x, y) \in T$.

Definition 6 *Let $u \in C^2(\overline{\Omega})$ be a function with symmetric positive definite Hesse matrix, $\mathcal{T}_h$ an ω-triangulation, $T_i \in \mathcal{T}_h$, and $\varepsilon_i(\omega)$ the ellipse given by (32). We say that T_i is an* optimal triangle *if*

$$T_i \subset \varepsilon_i(\omega) \tag{33}$$

and

$$\mathrm{meas}(T_i) \geq \mathrm{meas}(T) \textit{ for all triangles } T \subset \varepsilon_i(\omega). \tag{34}$$

Lemma 3 *Let $u \in C^2(\overline{\Omega})$ be a function with symmetric positive definite Hesse matrix. Further, let $\omega > 0$ be given, let $(x_i, y_i) \in \Omega$ and $\varepsilon_i(\omega)$ be the ellipse defined by (32). Then there exist four different triangles T_i^j, $j = 1, \ldots, 4$ with the center of gravity (x_i, y_i) satisfying (33) and (34) (see Figure 3).*

Proof. See [14]. □

If T_i is the optimal triangle for every $T_i \in \mathcal{T}_h$ then $E_{\mathrm{I}}(x, y) \leq \omega$ for every $(x, y) \in \Omega \cap \Omega_h$. Therefore $\mathcal{T}_h$ is the ω-triangulation and due to (34) $\mathcal{T}_h$ has reasonably small number of elements and approximates $\mathcal{T}_h^{\min}$ well.

In order to describe the optimal triangle geometrically we introduce the following

Definition 7 *Let $\boldsymbol{M}$ be a 2×2 symmetric positive definite matrix and $\boldsymbol{v} \in I\!R^2$. We define* the norm *of the vector $\boldsymbol{v}$* corresponding *to the matrix $\boldsymbol{M}$ as*

$$\|\boldsymbol{v}\|_{\boldsymbol{M}} \equiv \left(\boldsymbol{v}\boldsymbol{M}\boldsymbol{v}^T\right)^{\frac{1}{2}}. \tag{35}$$

Remark 2 *If $\boldsymbol{M} = \boldsymbol{I}$ (=identity matrix) then $\|\boldsymbol{v}\|_{\boldsymbol{M}} = \|\boldsymbol{v}\|_E$, where $\|\boldsymbol{v}\|_E$ is the Euclidean norm of $\boldsymbol{v}$.*

Lemma 4 *Let $u \in C^2(\overline{\Omega})$ be a function with symmetric positive definite Hesse matrix $\boldsymbol{H}(u(x,y))$, $(x,y) \in \Omega$, $\mathcal{T}_h$ a triangulation of Ω, $T_i \in \mathcal{T}_h$ with center of gravity (x_i, y_i), and $\varepsilon_i(\omega)$ the ellipse given by (32). Let V_i^j, $j = 1,2,3$, be vertices of T_i. Then T_i is the optimal triangle if and only if*

$$\|V_i^1 - V_i^2\|^2_{\boldsymbol{M}} = \|V_i^2 - V_i^3\|^2_{\boldsymbol{M}} = \|V_i^3 - V_i^1\|^2_{\boldsymbol{M}} = 6\omega, \tag{36}$$

where we put $\boldsymbol{M} = \boldsymbol{H}(u(x_i, y_i))$.

Proof. See [14]. □

Remark 3 *The assumption of positive definiteness of the Hesse matrix can be weakened. We do not do this in order to be compatible with our previous results in this field to which we refer above.*

3 Anisotropic Mesh Adaptation Method

Definition 7 and Lemma 4 give us a suitable tool for the practical construction of the triangulation $\mathcal{T}_h^{\min}$. On the other hand the condition (36) for $i = i_1, i_2$ cannot be generally satisfied for two triangles $T_{i_1} \neq T_{i_2}$ with the common edge $\partial T_{i_1} \cap \partial T_{i_2} \neq \emptyset$. To avoid these difficulties we pass from the center of gravity associated Hesse matrices to the edge associated Hesse matrices. This edge associated approach is simpler for numerical implementation.

3.1 Optimal triangulation

Definition 8 *Let $u \in C^2(\overline{\Omega})$ be a function with symmetric positive definite Hesse matrix and let $\omega > 0$ be given. Let $\mathcal{T}_h$ be a triangulation of the computational domain Ω. Let $\boldsymbol{H}_k$ be the Hesse matrix of u evaluated at the centre of the edge S_k, $k \in K$(= an index set), of the triangulation $\mathcal{T}_h$. We say that the triangulation $\mathcal{T}_h$ is* edge-optimal, *if*

$$\|S_k\|_{\boldsymbol{H}_k} = \sqrt{6\omega} \qquad \forall k \in K. \tag{37}$$

Remark 4 *The matrix $\boldsymbol{H}_k$ can be interpreted as an* interpolation error matrix *and the norm $\|S_k\|_M$ as an* interpolation error over the edge *S_k (see [7], [21]). It means that the interpolation error (considered in terms of $\|\cdot\|_{\boldsymbol{H}_k}$) for each edge of $\mathcal{T}_k$ is uniformly distributed over the triangulation.*

Remark 5 *It is easy to show ([14]), that the edge-optimal triangulation exists only for special cases. It lead us to a weaker form of the concept of edge-optimal triangulation. We introduce the quality parameter $Q_{\mathcal{T}_h}$ which measures the edge-optimality in the least squares sense.*

Definition 9 *Let $u \in C^2(\overline{\Omega})$ be a function with symmetric positive definite Hesse matrix and let $\omega > 0$ be given. Let $\mathcal{T}_h$ be a triangulation of the computational domain Ω. Let $\boldsymbol{H}_k$ be the Hesse matrix of u evaluated at the centre of the edge S_k, $k \in K$ (= an index set), of the triangulation $\mathcal{T}_h$. We say that the triangulation $\mathcal{T}_h^{\mathrm{opt}}$ is* **optimal** *if*

$$Q_{\mathcal{T}_h^{\mathrm{opt}}} = \min Q_{\mathcal{T}_h}, \tag{38}$$

where the minimum is taken over all triangulations of Ω and

$$Q_{\mathcal{T}_h} = \frac{1}{\#\mathcal{T}_h} \sum_{k \in K} \left(\|S_k\|_{\boldsymbol{H}_k} - \sqrt{6\omega} \right)^2, \tag{39}$$

where $\#\mathcal{T}_h$ is the number of edges of $\mathcal{T}_h$. We call the quantity $Q_{\mathcal{T}_h}$ the quality parameter *of $\mathcal{T}_h$.*

3.2 Optimization of the mesh

For a given $\mathcal{T}_h$ the quality parameter $Q_{\mathcal{T}_h}$ is a computable quantity. We adapt the triangulation $\mathcal{T}_h$ in order to decrease $Q_{\mathcal{T}_h}$ and to approach $\mathcal{T}_h^{\mathrm{opt}}$ and so $\mathcal{T}_h^{\mathrm{min}}$. Let $\partial\Omega$ denote boundary of the domain Ω. Let $u \in C^2(\overline{\Omega})$, $\omega > 0$, $\mathcal{T}_{\mathrm{old}}$ be a triangulation of Ω and $\boldsymbol{H}_k$, $k \in K$, be the Hesse matrices of u evaluated at the centre of the edge S_k. The triangulation contains two types of nodes: I (for internal) and B (for boundary). An II edge is an edge that joins two I nodes and the other combinations are defined analogously. We want to find a new triangulation $\mathcal{T}_{\mathrm{new}}$ such that $Q_{\mathcal{T}_{\mathrm{new}}}$ is minimal for all possible triangulations. To obtain $\mathcal{T}_{\mathrm{new}}$, an iterative process is used. Each iteration consists of a certain number of the following local operations (see Figure 4):

- **Adding a node** ($\mathcal{A}$) - If the norm of some edge of a triangle is greater than $\sqrt{32\omega/3}$ (see [14]) then we put a new node.
  - *II or IB edge*: we put a new node at the center of this edge.
  - *BB edge*: a new node is the orthogonal projection of the center of this edge on $\partial\Omega$.
- **Removing an edge** ($\mathcal{R}$) - If the norm of some edge of a triangle is smaller than $\sqrt{8\omega/3}$ (see [14]) we remove this edge. The initial and final nodes of this edge pass into a new node whose position depends on the type of edge.
  - *II edge*: the new position is at the center of the removed edge.
  - *IB edge*: the new position is at the position of the B node
  - *BB edge*: the new position is at the orthogonal projection of the center of the removed edge on $\partial\Omega$.
- **Swapping**($\mathcal{S}$) the diagonal of the quadrilateral formed by any pair of adjacent elements. The edge is swapped if the quality parameter $Q_{\mathcal{T}}$ after swapping is smaller than before.
- **Moving a node** ($\mathcal{M}$) is the only nondiscrete local operation. We seek a new position of a node (positions of other nodes are fixed) which minimizes the quality parameter $Q_{\mathcal{T}}$.

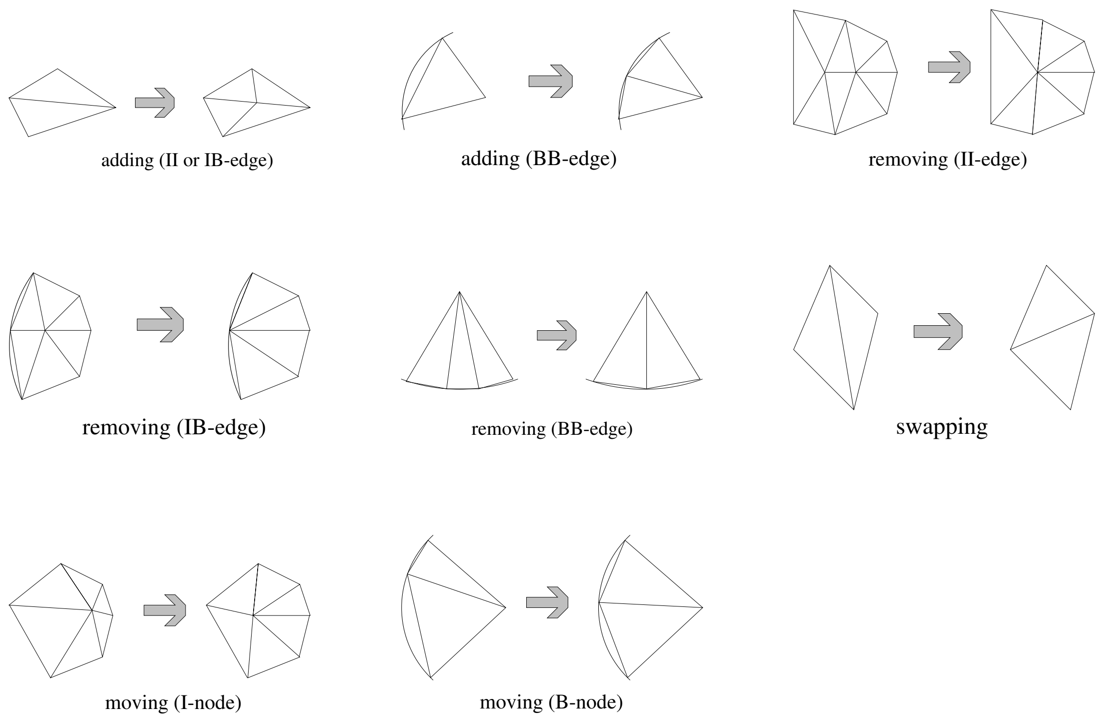

Figure 4: Local operations used in AMA algorithm.

- *I node*: we construct a weighted center of gravity of triangles containing the node as a vertex and the node is moved towards the weighted center of gravity till the quality parameter $Q_{\mathcal{T}}$ decreases (see [14]).
- *B node*: we move the node along $\partial\Omega$ and the new position minimizes the quality parameter $Q_{\mathcal{T}}$.

3.3 Iterative process

In [14] we presented the AMA algorithm using the combination of the above operations $\mathcal{A}, \mathcal{R}, \mathcal{S}$, and $\mathcal{M}$ as

$$m \times [\mathcal{M} + \mathcal{S} + \mathcal{R} + \mathcal{M} + \mathcal{A} + \mathcal{M} + \mathcal{S}] + \mathcal{M} \tag{40}$$

(the sequence of operations goes from the left to the right), where m is an integer denoting the number of repetitions of the sequence of operations in the square brackets. The sequence in the square brackets is applied until no local discrete operation $\mathcal{S}$, $\mathcal{R}$ and $\mathcal{A}$ are performed.

In this paper we improved the formula (40) to a new formula

$$m \times \{\mathcal{M} + n_1 \times [\mathcal{R} + \mathcal{S}] + \mathcal{M} + n_2 \times [\mathcal{A} + \mathcal{S}] + M + \mathcal{S}\} + \mathcal{M}, \tag{41}$$

where n_1 and n_2 have the same meaning as m in (40). In what follows the sequence of operations (41) is used.

4 Application of AMA in numerical solution process

In the previous section we showed how to construct, for the exact sufficiently smooth solution u of a BVP, a triangulation $\mathcal{T}_h^{\mathrm{opt}}$ suitable for its numerical solution. In practical examples, of course, we do not know the exact solution u and therefore we use a numerical approximation u_h on a mesh $\mathcal{T}_h$, on which we apply a smoothing procedure and use the technique from previous section. What we need is not the smoothed function itself but its Hesse matrices $\boldsymbol{H}$ evaluated at the centres of edges of $\mathcal{T}_h$.

4.1 Computation of the second order derivatives

The Hesse matrix $\boldsymbol{H}$ evaluated at the centre of an edge S_k of $\mathcal{T}_h$ is computed as the average of the Hesse matrices evaluated at the initial and final point forming S_k. Let $u_h \in U_h$ (defined in (16)) be an approximate solution of (4) – (6) and

$$\begin{aligned} W_h &= \{w_h; w_h \in C(\overline{\Omega_h}), w_h \text{ is linear on each } T \in \mathcal{T}_h\}, \\ W_h^0 &= \{w_h; w_h \in W_h, w_h = 0 \text{ on } \partial\Omega_h\}. \end{aligned} \tag{42}$$

We introduce the operator $u_h \in U_h \mapsto \bar{u}_h \in W_h$ such that

$$\bar{u}_h(P_i) = \frac{\sum_{T\in D_i} \int_T u_h(\xi)\, d\xi}{\sum_{T\in D_i} \mathrm{meas}(T)}, \tag{43}$$

where $P_i \in \sigma_h$ (see Definition 1) and D_i is the set of triangles from $\mathcal{T}_h$ having P_i in common.

We compute the elements of the Hesse matrix $\boldsymbol{H}$ using the evaluation of second order derivatives of $\bar{u}_h$ in the following sense. We approximate $\partial^2\bar{u}_h/\partial x^2$ by a function $u_h^{xx} \in W_h$ such that

$$\left(\frac{\partial^2 \bar{u}_h}{\partial x^2}, \varphi\right) \approx (u_h^{xx}, \varphi) = -\left(\frac{\partial \bar{u}_h}{\partial x}\frac{\partial \varphi}{\partial x}\right) \quad \forall \varphi \in W_h^0, \tag{44}$$

where $(\cdot,\cdot)$ means the inner product in $L^2(\Omega_h)$. The R.H.S. of (44) has meaning because $\bar{u}_h, \varphi \in W_h$ and therefore the first derivatives exist and are piecewise constant. The choice of the standard finite element hat test functions from W_h^0 leads to the explicit formula for u_h^{xx}. The quantities u_h^{xy}, u_h^{yx} and u_h^{yy} approximating $\partial^2\bar{u}_h/\partial x\partial y$, $\partial^2\bar{u}_h/\partial y\partial x$ and $\partial^2\bar{u}_h/\partial y^2$, respectively, are computed analogously. For vertices lying on $\partial\Omega$ we use an extrapolation from the interior part of the computational domain. For more detail see [14], Section 6.1. We put

$$\boldsymbol{H} = \begin{pmatrix} u_h^{xx} & u_h^{xy} \\ u_h^{yx} & u_h^{yy} \end{pmatrix}. \tag{45}$$

Remark 6 *The matrix $\boldsymbol{H}$ given by (45) is symmetric ($u_h^{xy} = u_h^{yx}$, see [14], Section 6.1) but not positive definite as is required in previous sections. Moreover, if $\bar{u}_h$ is linear in Ω_h then $u_h^{xx} = u_h^{xy} = u_h^{yy} = 0$ in Ω. Therefore $\|S_k\|_{\boldsymbol{H}_k} = 0\ \forall k \in K$ and consequently $Q_{\mathcal{T}_h} = 6\omega$ in (39) for any triangulation $\mathcal{T}_h$ of Ω, and the iterative process from Section 3 cannot be applied to minimization of $Q_{\mathcal{T}_h}$. In this case it is natural to require the uniform mesh which can be obtained by setting $\boldsymbol{H}_k := c\boldsymbol{I}$, where $c > 0$ is a constant and $\boldsymbol{I}$ is a unit 2×2 matrix. For these reasons we use its modification $\boldsymbol{M}$ instead of $\boldsymbol{H}$. This means that the function $\bar{u}_h$ is smoothed by prescribing the conditions on the Hesse matrix resulting from the smoothing procedure which is the novelty of this paper.*

4.2 Generation of the matrices M

Let $\boldsymbol{H}(P_i)$, $P_i \in \sigma_h$, be a Hesse matrix (45) evaluated at the vertex P_i. As $\boldsymbol{H}(P_i)$ is symmetric we decompose it in the following way:

$$\boldsymbol{H}(P_i) = R_i \begin{pmatrix} \lambda_{i1} & 0 \\ 0 & \lambda_{i2} \end{pmatrix} R_i^{-1}, \quad i \in J, \tag{46}$$

where R_i, $i \in J$, are orthogonal matrices. As matrices $\boldsymbol{H}(P_i)$ are generally not positive definite we put

$$\bar{\boldsymbol{H}}(P_i) = R_i \begin{pmatrix} |\lambda_{i1}| & 0 \\ 0 & |\lambda_{i2}| \end{pmatrix} R_i^{-1}, \quad i \in J. \tag{47}$$

The matrices $\bar{\boldsymbol{H}}(P_i)$, $P_i \in \sigma_h$, are symmetric positive definite. To avoid the problems mentioned in Remark 6 we put

$$\boldsymbol{M}(P_i) = c\left[\boldsymbol{I} + \alpha(\|\bar{\boldsymbol{H}}(P_i)\|)\bar{\boldsymbol{H}}(P_i))\right], \quad P_i \in \sigma_h, \tag{48}$$

where $\boldsymbol{I}$ is a unit 2×2 matrix, $c > 0$ is a constant and $\alpha : \langle 0, \infty) \to \langle 0, \infty)$ is a function. In (48) we put $\|\bar{\boldsymbol{H}}\| = \max_{i,j=1,2} |\bar{h}_{ij}|$, where $\bar{h}_{ij}$, $i, j = 1, 2$, are the elements of $\boldsymbol{H}$. The first term in the square brackets of (48) guarantees that the matrices $\boldsymbol{M}(P_i)$ are always nonsingular.

4.2.1 Setting of parameter c

If $\boldsymbol{H}(P_i) = 0\ \forall P_i \in \sigma_h$ then $\boldsymbol{M}(P_i) = c\boldsymbol{I}\ \forall P_i \in \sigma_h$. If the edge-optimal triangulation from Definition 8 exists, then it consists of equal equilateral triangles. As $\boldsymbol{M}(P_i) = c\boldsymbol{I}\ \forall P_i \in \sigma_h$ then (37) yields

$$\|S_k\|^2_{\boldsymbol{H}(P_i)} = ch^2 = 6\omega \qquad \forall k \in K, \tag{49}$$

where h is the length of edges defined in (18), and then

$$h = \sqrt{\frac{6\omega}{c}}. \tag{50}$$

The area of the equilateral triangle T with the length of edge h is

$$\mathrm{meas}(T) = \frac{\sqrt{3}}{4} h^2. \tag{51}$$

In this case, the edge-optimal triangulation $\mathcal{T}_h$ of Ω consists of *numel* equal equilateral triangles, where

$$numel = \frac{\mathrm{meas}(\Omega)}{\mathrm{meas}(T)}. \tag{52}$$

This, (50), and (51) imply that

$$c = \frac{6\omega\sqrt{3}}{4} \frac{numel}{\mathrm{meas}(\Omega)} \tag{53}$$

and

$$h = \left(\frac{4\,\mathrm{meas}(\Omega)}{\sqrt{3}\,numel}\right)^{1/2}. \tag{54}$$

It means that for a given *numel* the relation (48) leads to the same triangulation $\mathcal{T}_h$ independently of $\omega > 0$ provided that $\boldsymbol{H}(P_i) = 0\ \forall P_i \in \sigma_h$. In order to keep our considerations compatible with results from [14] we set $\omega = 1/2$.

Having defined ω, the parameter c is set according to (53) as

$$c = \frac{3\sqrt{3}}{4} \frac{numel}{\mathrm{meas}(\Omega)}, \tag{55}$$

where *numel* is the number of triangles prescribed by user for the construction of the triangulation $\mathcal{T}_h$ (cf. [14], relation (32)). If the uniform triangulation should be constructed then the user controls by *numel* how many triangles the triangulation should contain.

4.2.2 Setting of α

The simplest way to define α is to put

$$\alpha(\|\bar{\boldsymbol{H}}(P_i)\|) = C,\ C = \mathrm{const},\ C > 0. \tag{56}$$

When solving problems with discontinuities (e.g. transonic flow with strong shocks), the norm $\|\bar{\boldsymbol{H}}(P_i)\|$ can tend to infinity for some $P_i \in \sigma_h$. Then the drawback of the choice (56) is that the condition

$$h^2 \le \bar{c}\,\mathrm{meas}(T),\ T \in \mathcal{T}_h,\ \bar{c} = \text{constant independent of } h, \tag{57}$$

is not satisfied as $\|\boldsymbol{H}(P_i)\| \to \infty$ for some $P_i \in \sigma_h$. The condition (57) is the standard requirement for the finite volume/element methods, see, e.g., [17]. To fulfil (57) we propose the relation

$$\alpha(\|\bar{\boldsymbol{H}}(P_i)\|) = \frac{\varepsilon_1}{\varepsilon_2 + \|\bar{\boldsymbol{H}}(P_i)\|}, \quad P_i \in \sigma_h, \tag{58}$$

where ε_1 and ε_2 are positive constants. The relations (48) and (58) give

$$\lim_{\|\bar{\boldsymbol{H}}(P_i)\| \to \infty} \|\boldsymbol{M}(P_i)\| = c(1 + \varepsilon_1), \quad P_i \in \sigma_h, \tag{59}$$

from which it follows that the norms of $\boldsymbol{M}(P_i)$, $P_i \in \sigma_h$, are bounded and, therefore, the lengths of edges of $\mathcal{T}$ are bounded from below. The relation (58) is used in further computation.

The parameters $\varepsilon_1, \varepsilon_2$ are determined in the following way. Let $\bar{\boldsymbol{H}}(P_i) = 0$ for some $P_i \in \sigma_h$. Then $\boldsymbol{M}(P_i) = c\boldsymbol{I}$ and the corresponding optimal triangle has equal edges of length (in Euclidean norm)

$$l_{\max} = \sqrt{\frac{3}{c}}. \tag{60}$$

Let $\bar{\boldsymbol{H}}(P_i) = \beta \boldsymbol{I}$ for some $P_i \in \sigma_h$ and let $\beta \gg 1$. Then $\boldsymbol{M}(P_i) \to c(1 + \varepsilon_1)\boldsymbol{I}$ for $\beta \to \infty$, as follows from (59), and the corresponding optimal triangle has equal edges of limit length (in Euclidean norm)

$$l_{\min} = \sqrt{\frac{3}{c(1 + \varepsilon_1)}}. \tag{61}$$

It follows from (60) and (61) that the length l of any edge from the edge-optimal triangulation satisfies (provided $\boldsymbol{M}(P_i)$ is defined by (48) and (58))

$$l_{\min} = \sqrt{\frac{3}{c(1 + \varepsilon_1)}} \le l \le \sqrt{\frac{3}{c}} = l_{\max}. \tag{62}$$

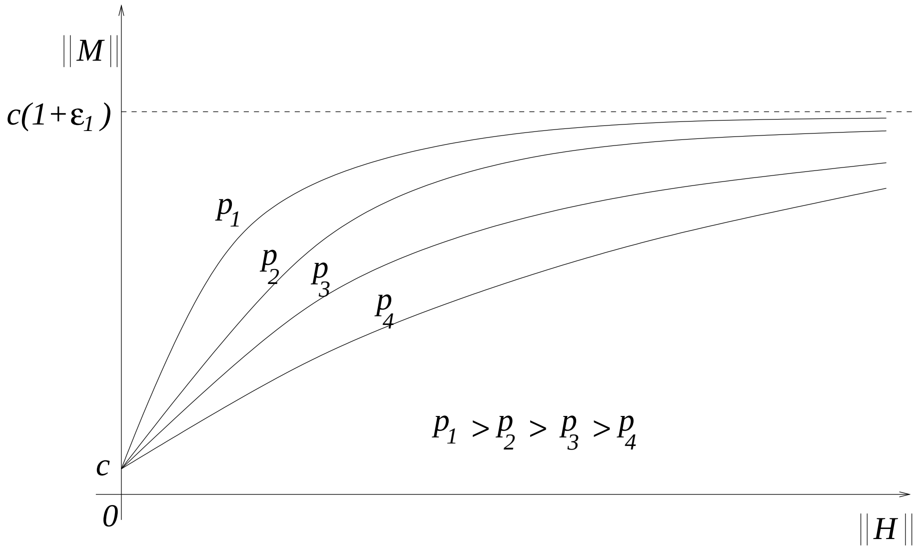

Figure 5: Dependence of $\|\boldsymbol{M}\|$ on $\|\bar{\boldsymbol{H}}\|$ for different p.

It follows from (60) and (61) that

$$\frac{l_{\max}}{l_{\min}} = \sqrt{1+\varepsilon_1} \tag{63}$$

and then

$$\varepsilon_1 = \left(\frac{l_{\max}}{l_{\min}}\right)^2 - 1. \tag{64}$$

Relation (64) explains the role of ε_1. Setting ε_1 we control the ratio between the longest and the shortest edge admissible in the edge-optimal triangulation.

In the practical computation we use for ε_2 the following relation

$$\varepsilon_2 = \frac{\varepsilon_1}{p}, \tag{65}$$

where p is some positive number. The role of p is viewed in Figure 5, where the function

$$\|\bar{\boldsymbol{H}}\| \mapsto \|\boldsymbol{M}\| = c\left(1 + \frac{\varepsilon_1}{\frac{\varepsilon_1}{p} + \|\bar{\boldsymbol{H}}\|}\|\bar{\boldsymbol{H}}\|\right) \tag{66}$$

is plotted for different p. The number p controls the transition of the coarsest part of the mesh (with edge length l_{max} given by (60)) to the finest one (with edge length l_{min} given by (61)) as it is demonstrated in Figure 6.

4.3 Multilevel computation

The technique described above is applied in the following way: We start from an initial triangulation $\mathcal{T}_{h_0}$ of the computational domain Ω. We compute the solution u_{h_0} on the triangulation $\mathcal{T}_{h_0}$ using a suitable numerical method (finite volume method, finite element method, ...) for the approximate solution of the problem (1) – (3). We compute the Hesse matrices $\boldsymbol{M}$ by the technique described above at each vertex of $\mathcal{T}_{h_0}$ and we construct the

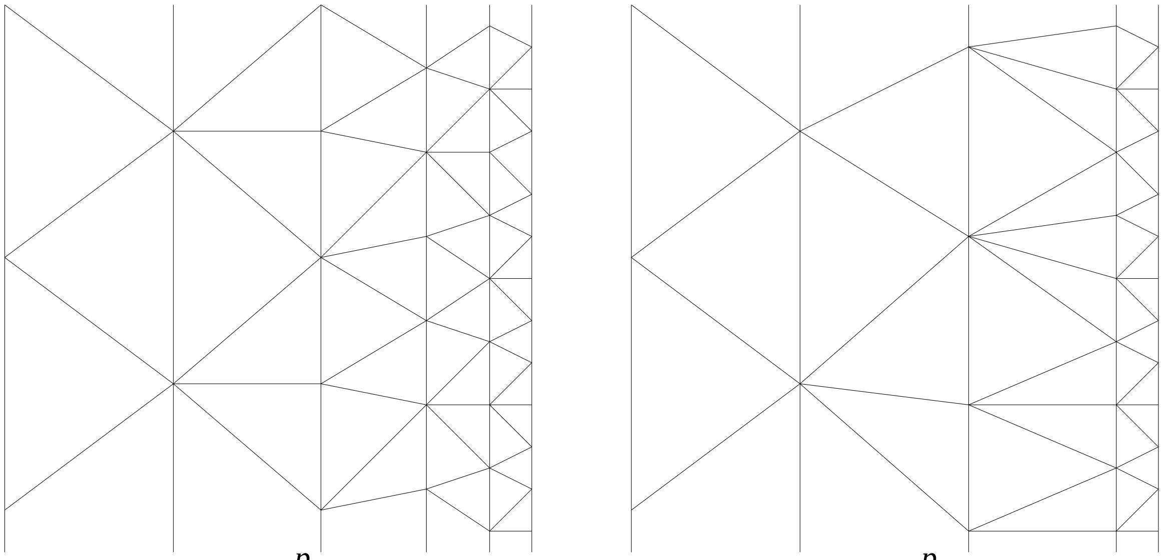

Figure 6: Transition of the coarsest part to the finest one for two different $p_1 > p_2$.

triangulation $\mathcal{T}_{h_1}$ using the iterative process (41). The results from $\mathcal{T}_{h_0}$ are interpolated onto $\mathcal{T}_{h_1}$ and the numerical solution procedure is applied to $\mathcal{T}_{h_1}$ producing u_{h_1}. In a similar way we construct $\mathcal{T}_{h_2}, u_{h_2}; \mathcal{T}_{h_3}, u_{h_3}; \ldots$. The multilevel computational process is terminated on the mesh $\mathcal{T}_{h_k}$ if two successive triangulations $\mathcal{T}_{h_k}$ and $\mathcal{T}_{h_{k+1}}$ are (approximately) identical.

5 Computational results

In the previous section we described the construction of a new triangulation if the matrices $\boldsymbol{M}(P_i), P_i \in \sigma_h$ are given. To define $\boldsymbol{M}(P_i)$ we use the relations (46) – (48), (53), (58), and (65), where the meaning of constants *numel*, ε_1, and p is specified in Section 4.2. Their determination is demonstrated on the two following numerical examples.

The value *numel* represents the number of triangles in the initial mesh before the first adaptation. Let $\bar{l}$ be a characteristic length of a given domain. It is sufficient that the step size h of the mesh is z times smaller then $\bar{l}$ where we take z from the interval $\langle 1, 10 \rangle$. The area of the equilateral triangle with length of edge h is equal to $\sqrt{3}h^2/4$. Taking into account the relation

$$numel \frac{\sqrt{3}}{4} \left(\frac{\bar{l}}{z} \right)^2 \approx \mathrm{meas}(\Omega), \tag{67}$$

we put

$$numel := \frac{4}{\sqrt{3}} \left(\frac{z}{\bar{l}} \right)^2 \mathrm{meas}(\Omega). \tag{68}$$

Therefore, we can choose the value *numel* according to (68). Numerical experiments show that the choice (68) is suitable.

To set the constants ε_1 and p we have applied AMA first to scalar elliptic equations (see [6]), where the exact solutions are known.

5.1 A singular diffusion problem

In [6] the following problem is formulated. Find $u : \overline{\Omega} \to I\!R^1$ satisfying

$$\Delta u = 0 \qquad \text{in } \Omega, \tag{69}$$

where

$$\Omega = \Big\{(x,y) \in I\!R^2, x^2 + y^2 < 1\Big\} \setminus \Big\{(x,y) \in I\!R^2, x \in (0,1), y = 0\Big\} \tag{70}$$

is the unit circle with a "crack" along the positive x axis. The boundary conditions are $u = \sin(\theta/4)$ along the unit circumference (θ being the angle with respect to the positive x axis), $u = 0$ along the upper surface of the crack, and $\partial u/\partial n = 0$ along the lower surface of the crack. The exact solution of the weak problem is

$$u(r,\theta) = r^{1/4} \sin(\theta/4) \tag{71}$$

(r and θ are the polar coordinates) which belongs to $H^1(\Omega) \setminus H^2(\Omega)$, with a singularity at the origin. If h denotes the longest edge size in the triangulation, it is a classical result ([6], p. 4126) that

$$|\!|\!| u - u_h |\!|\!| \equiv \|\nabla(u - u_h)\|_{L^2(\Omega)} \leq \beta h^\kappa \tag{72}$$

with $\kappa < \frac{1}{4}$ (remember that for regular problems ($u \in H^2(\Omega)$) $\kappa = 1$, see [17], 2.9.41). Here u denotes the exact solution and u_h the piecewise linear finite element numerical solution of (69).

5.1.1 Uniform meshes

First we have solved (69) using uniform meshes. The important effect of the AMA algorithm is that it can be used as a uniform mesh generator. To this end we start on a very coarse mesh and apply the AMA algorithm described in Section 2 with isotropic metric, i.e. with $\boldsymbol{M}(P_i) = c\boldsymbol{I},\ P_i \in \sigma_h$, where c is the constant given by (55), where we prescribe the number of elements *numel*.

To solve the equation (69) we applied the standard finite element method (FEM) with conforming piecewise linear elements. Therefore, the approximate solution u_h is sought in the space

$$U_h = \{u_h \in C(\Omega_h); u_h|_T \in P_1(T)\ \forall T \in \mathcal{T}_h, u_h|_{\Gamma_D} = u_D\}, \tag{73}$$

where $\Gamma_D \subset \partial\Omega$ is the part of the boundary where the Dirichlet boundary condition u_D is prescribed.

Let $u_h \in U_h$ be the approximate solution of the discrete version of the problem (69) computed on triangulation $\mathcal{T}_h$. As we know the exact solution (71), we compute the error (70)

$$e_h \equiv |\!|\!| u - u_h |\!|\!| = \left(\sum_{T \in \mathcal{T}_h} \int_T |\nabla(u(x) - u_h(x))|^2 \, dx\right)^{1/2}, \tag{74}$$

where the integral is evaluated by the seven point numerical quadrature exact for polynomials of degree less than or equal to 3.

We define the operator Π_h using (11) where we put $\|\cdot\|_X = |\!|\!|\cdot|\!|\!|$, i.e. $\Pi_h : w \in H^1(\Omega) \mapsto \Pi w \in U_h$ such that

$$|\!|\!| w - \Pi_h w |\!|\!| = \min_{w_h \in U_h} |\!|\!| w - w_h |\!|\!|. \tag{75}$$

numel	*nelem*	h	e_h	$e_h^{\min}$	CPU (s)
125	156	0.3079	1.0120	0.8094	7
500	628	0.1540	0.8333	0.6914	9
2000	2442	0.0789	0.7159	0.5958	23
8000	9831	0.0395	0.5837	0.4954	154
32000	39158	0.0199	0.4707	0.4036	2408

Table 1: Singular diffusion problem – uniform meshes.

Using the standard technique for seeking the minimum of a function of several variables, it is possible to show that for each $w \in H^1(\Omega)$ there exists a uniquely determined function $\Pi_h w \in U_h$. Then we can compute the *minimal discretization error*

$$e_h^{\min} \equiv |||u - \Pi_h u||| = \left(\sum_{T \in \mathcal{T}_h} \int_T |\nabla(u(x) - \Pi_h u(x))|^2 \, dx \right)^{1/2}. \tag{76}$$

The function $\Pi_h u$ can be interpreted as the *best possible numerical solution* in the space U_h in the sense of error measured in the $|||\cdot|||$ norm for a given triangulation.

Table 1 contains the results of computation on five different uniform meshes. The value *numel* is the number of prescribed elements in (55) and *nelem* is the real number of triangles of generated triangulation. The number h in Table 1 denotes the step size of a uniform mesh

$$h \equiv \max_{T \in \mathcal{T}_h} \operatorname{diam}(T). \tag{77}$$

The values e_h and $e_h^{\min}$ are given by (74) and (76), respectively. The last column introduces the CPU time including the mesh generation process. The computation was performed on DEC Alpha EV56/500MHz workstation.

Using the data from Table 1 we can compute the order of convergence. Let us suppose that

$$e_h = \beta h^{\kappa}, \tag{78}$$

where e_h is the discretization error given by (74), h the step size of the mesh given by (77), β a positive constant and κ the *order of convergence*. To compute κ we apply the *method of least squares* (for more detail see, e.g., [19]). Therefore, we obtain $\kappa = 0.28$ and $\beta = 1.49$, which corresponds with the theoretical result (72).

The smallest value of $e_h = 0.4707$ (computed for *numel* $= 32000$) is in agreement with the low order of convergence κ. We can easily estimate how many triangles would be required so that the discretization error would be significantly small, e.g. $e_h = 0.057$ (=the smallest error obtained with AMA, see Section 5.1.2, Table 2). From the computed values $\kappa = 0.28$ and $\beta = 1.49$ and the relation (78), we obtain $h = 3.5 \cdot 10^{-15}$, which corresponds approximately to $5.8 \cdot 10^{29}$ equilateral triangles.

5.1.2 Anisotropic meshes

Applying the AMA method we get more suitable meshes for the resolution of (69) in the sense that the minimal discretization error $e_h^{\min}$ is smaller than for uniform meshes. As we know the exact solution we can compare the matrices $\boldsymbol{M}(P_i)$ from Section 2 computed using the Hesse matrices of the exact and approximate solution, respectively. After simple but time consuming calculation we have

$$\bar{\boldsymbol{H}}(P_i) = \frac{3}{16} r_i^{-7/4} \boldsymbol{I}, \tag{79}$$

where $\boldsymbol{I}$ is the unit matrix and r_i is the radius of P_i.

In Section 4.2.2 we mentioned two possibilities of the setting of the function α. Now we focus on them:

1. Let $\alpha(\|\bar{\boldsymbol{H}}(P_i)\|)$ be given by (56). Then the edge-optimal triangulation consists of almost equilateral triangles (provided that $\mathrm{diam}(T) \ll r_T$) whose areas depend on the radius of their barycentres r_T according to

$$\mathrm{meas}(T) \approx \frac{3\sqrt{3}}{4} \left[c \left(1 + \frac{3}{16} C r_T^{-7/4} \right) \right]^{-1}. \tag{80}$$

   It follows from (80) that for $r_T \to 0$ the triangles of the optimal triangulation collapse, i.e., $\mathrm{meas}(T) \to 0$ and the condition (57) is not satisfied.

2. Let $\alpha(\|\bar{\boldsymbol{H}}(P_i)\|)$ be given by (58). Then for $\varepsilon_1 \gg 1$ we have

$$\mathrm{meas}(T) \approx \frac{3\sqrt{3}}{4} \left[c \left(1 + \frac{\frac{3}{16} p \varepsilon_1 r_T^{-7/4}}{\varepsilon_1 + \frac{3}{16} p r_T^{-7/4}} \right) \right]^{-1}, \tag{81}$$

   which for $r_T \to 0$ gives

$$\mathrm{meas}(T) \to \frac{3\sqrt{3}}{4} \frac{1}{c(1+\varepsilon_1)} \tag{82}$$

   and the condition (57) is satisfied.

From this point of view (58) seems to be better than (56). The numerical confirmation of these arguments was performed for several values of ε_1 and p.

To solve (69) we use the same numerical scheme as for uniform meshes. We performed the mesh adaptation for various combinations of values of ε_1 and p, see Table 2. The meaning of values in Table 2 is similar as in Table 1, *nelem* means the real number of elements after the last mesh adaptation and CPU is the time cost for all levels of adaptation including mesh generation.

Figure 7 shows the dependence of $h_T \equiv \mathrm{diam}(T)$, $T \in \mathcal{T}_h$, on r_T for the triangulation generated with $\varepsilon_1 = 10^{30}$ and $p = 200$. The single dots present the dependence of diameter h_T of each $T \in \mathcal{T}_h$ on its corresponding r_T while the dashed line presents the theoretical dependence given by

$$h_T = \frac{4}{\sqrt{3}} \left(\mathrm{meas}(T) \right)^{1/2}, \tag{83}$$

where $\mathrm{meas}(T)$ is given by (81). The good mutual correspondence is evident.

Figure 8 and Figure 9 show two examples of results from Table 2. The left-hand parts of figures present the used triangulation and the right-hand ones the corresponding lines of constant values of the numerical solution u_h together with the best possible numerical solution $\Pi_h u$. The second and third rows of figures represent 10 times and 100 times zooms of the neighbourhood of the singularity point, respectively.

$numel$	ε_1	p	$nelem$	e_h	$e_h^{\min}$	CPU (s)	
10	10^{10}	50	759	0.1481	0.1376	122	Figure 8
10	10^{20}	50	745	0.1378	0.1336	122	
10	10^{30}	50	745	0.1378	0.1336	128	
10	10^{10}	100	1577	0.1101	0.1022	245	
10	10^{20}	100	1610	0.0860	0.0841	247	
10	10^{30}	100	1598	0.0942	0.0880	222	
10	10^{10}	150	2404	0.0992	0.0906	405	
10	10^{20}	150	2464	0.0683	0.0673	426	
10	10^{30}	150	2452	0.0669	0.0656	400	
10	10^{10}	200	3194	0.0944	0.0835	610	
10	10^{20}	200	3375	0.0567	0.0554	666	
10	10^{30}	200	3376	0.0567	0.0554	649	Figure 9

Table 2: Singular diffusion problem – anisotropic mesh adaptation.

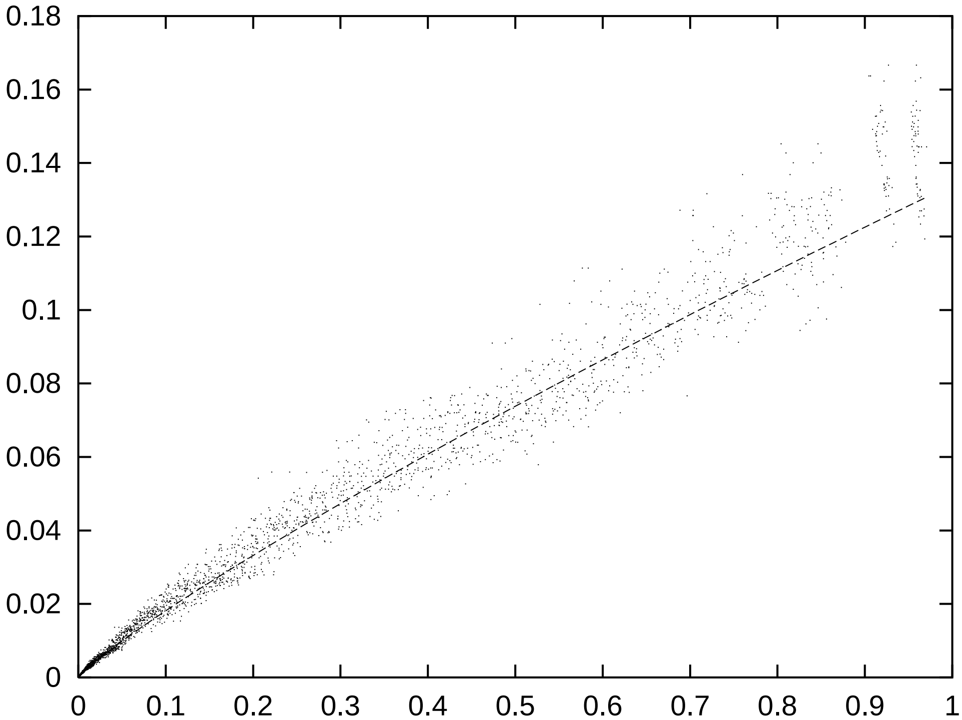

Figure 7: Singular diffusion problem – dependence of $h(T)$ on r_T for $\varepsilon_1 = 10^{30}$ and $p = 200$.

η	No. of ref.	*nelem*	e_h	$e_h^{\min}$	CPU (s)	
2E-04	8	1474	0.2175	0.1906	50	
2E-04	10	1538	0.1658	0.1485	66	
2E-04	12	1602	0.1330	0.1225	82	Figure 10
1E-04	8	2127	0.2121	0.1843	78	
1E-04	10	2181	0.1585	0.1403	102	
1E-04	12	2255	0.1237	0.1122	128	

Table 3: Singular diffusion problem – red-green refinement.

5.1.3 Isotropic mesh refinement

To demonstrate the efficiency of the AMA method, we solved (69) with the standard red-green refinement (RGR) technique [4]. Therefore we define the *error indicator*, cf. (74),

$$g(T) = \left(\int_T |\nabla u(x,y) - \nabla u_h(x,y)|^2 \, \mathrm{d}x \, \mathrm{d}y\right)^{1/2}, \quad T \in \mathcal{T}_h, \tag{84}$$

where u and u_h are the exact and numerical solutions, respectively. The error indicator (84) is one of the "best possible" indicators as it is based on the direct computation of the error (the exact solution is known).

All triangles $T \in \mathcal{T}_h$ with $g(T)$ greater than a given tolerance η are refined by the red-green technique [4]. The computation was performed for 2 values of the tolerance η and for 8, 10, and 12 levels of the mesh refinement. It is necessary to prescribe the number of levels of refinement as the singularity causes that there exist some triangles with $g(T) > \eta$ for any level of refinement. The achieved results are viewed in Table 3 and one of them is visualized in Figure 10.

5.2 A Poisson problem with steep gradients

The previous test, though essential for checking the convergence properties of the adaptive algorithm, allows no evaluation of the performance of the optimizer in relation to anisotropy. For problem (69), both eigenvalues of the Hesse matrix of the solution (71) differ only by sign (i.e. $\lambda_1 = -\lambda_2$) and thus the optimal triangulation consists of equilateral triangles.

Consider now a diffusion problem exhibiting steep gradients. Let $\Omega = (0,1) \times (0,1)$ and let u be the solution of

$$-\Delta u = 90x^8(1 - y^{20}) + 380y^{18}(1 - x^{10}) \tag{85}$$

with boundary conditions $u = 0$ along the edges $\{(x,y) \in I\!R^2; x = 1, \ y \in (0,1)\}$ and $\{(x,y) \in I\!R^2; x \in (0,1), \ y = 1\}$ and $\partial u/\partial n = 0$ along $\{(x,y) \in I\!R^2; x = 0, \ y \in (0,1)\}$ and $\{(x,y) \in I\!R^2; x \in (0,1), \ y = 0\}$. The exact solution

$$u = (1 - x^{10})(1 - y^{20}) \tag{86}$$

exhibits two steep gradients along the right-hand and top edges, the latter being stronger than the former.

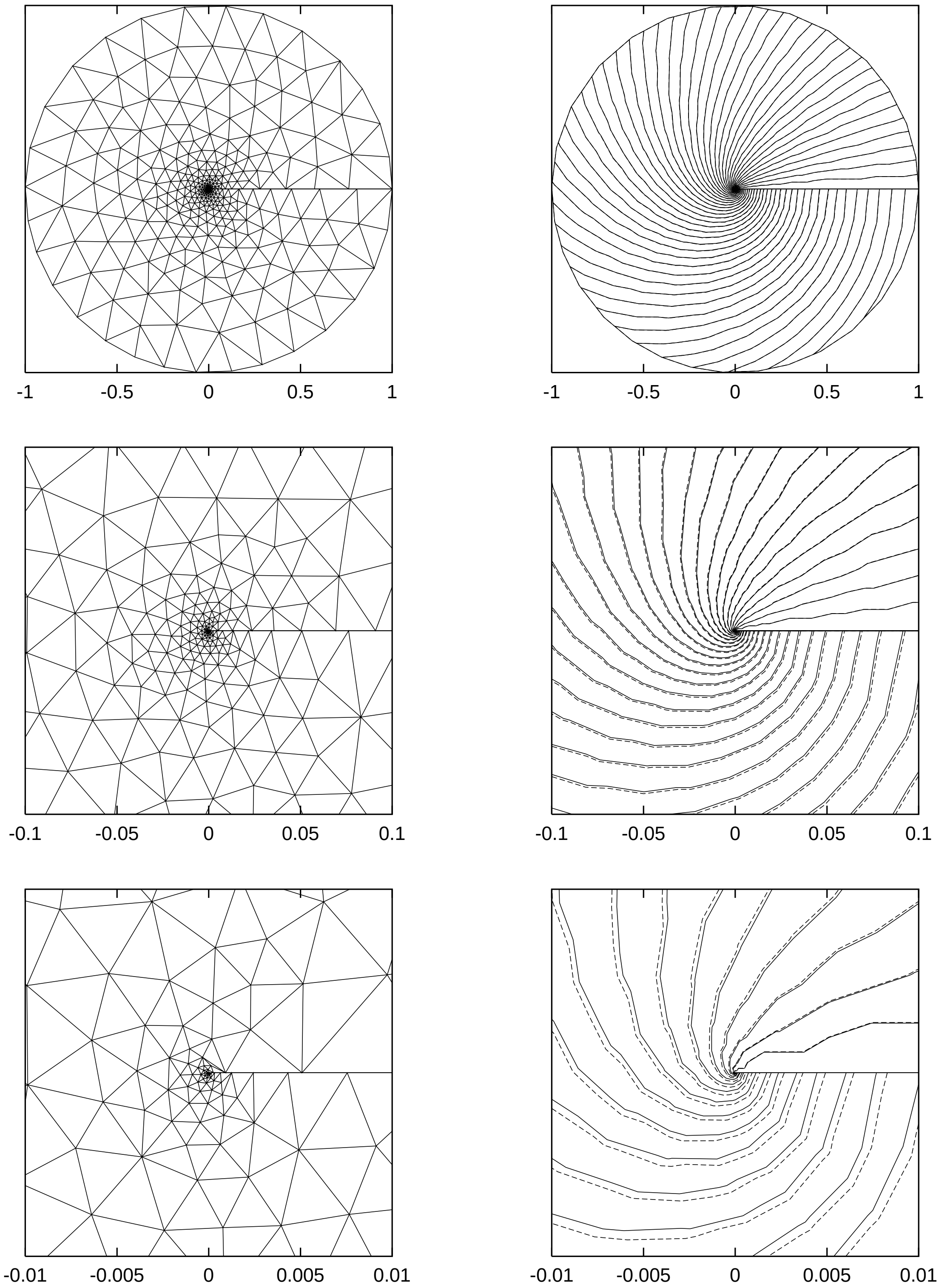

Figure 8: Singular diffusion problem, anisotropic mesh adaptation with $numel = 10$, $\varepsilon_1 = 10^{10}$, $p = 50$ ($nelem = 759$) – mesh and isolines of u_h (full line) and $\Pi_h u$ (dashed line) with zooms.

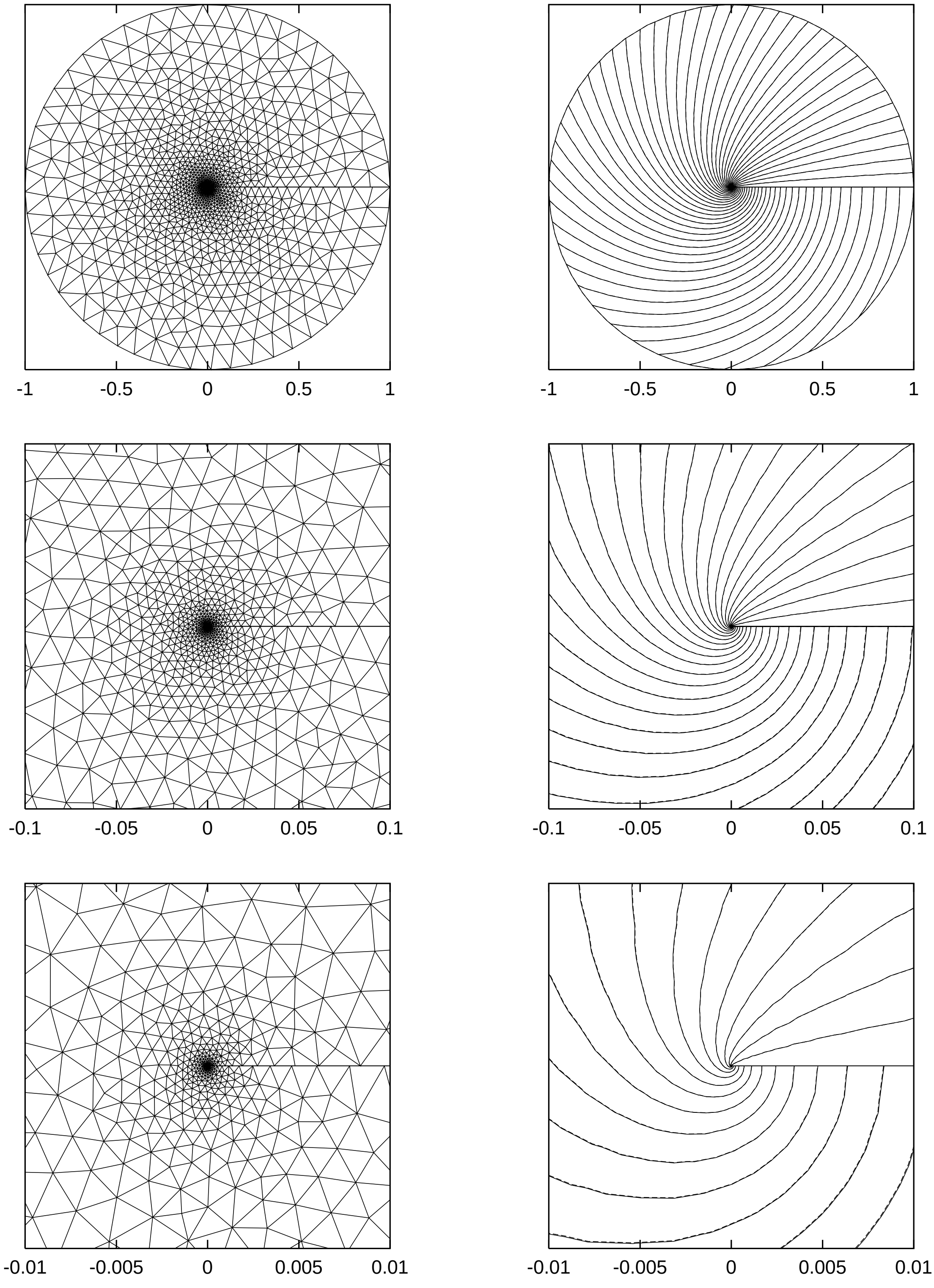

Figure 9: Singular diffusion problem, anisotropic mesh adaptation with $numel = 10$, $\varepsilon_1 = 10^{30}$, $p = 200$ ($nelem = 3376$) – mesh and isolines of u_h (full line) and $\Pi_h u$ (dashed line) with zooms.

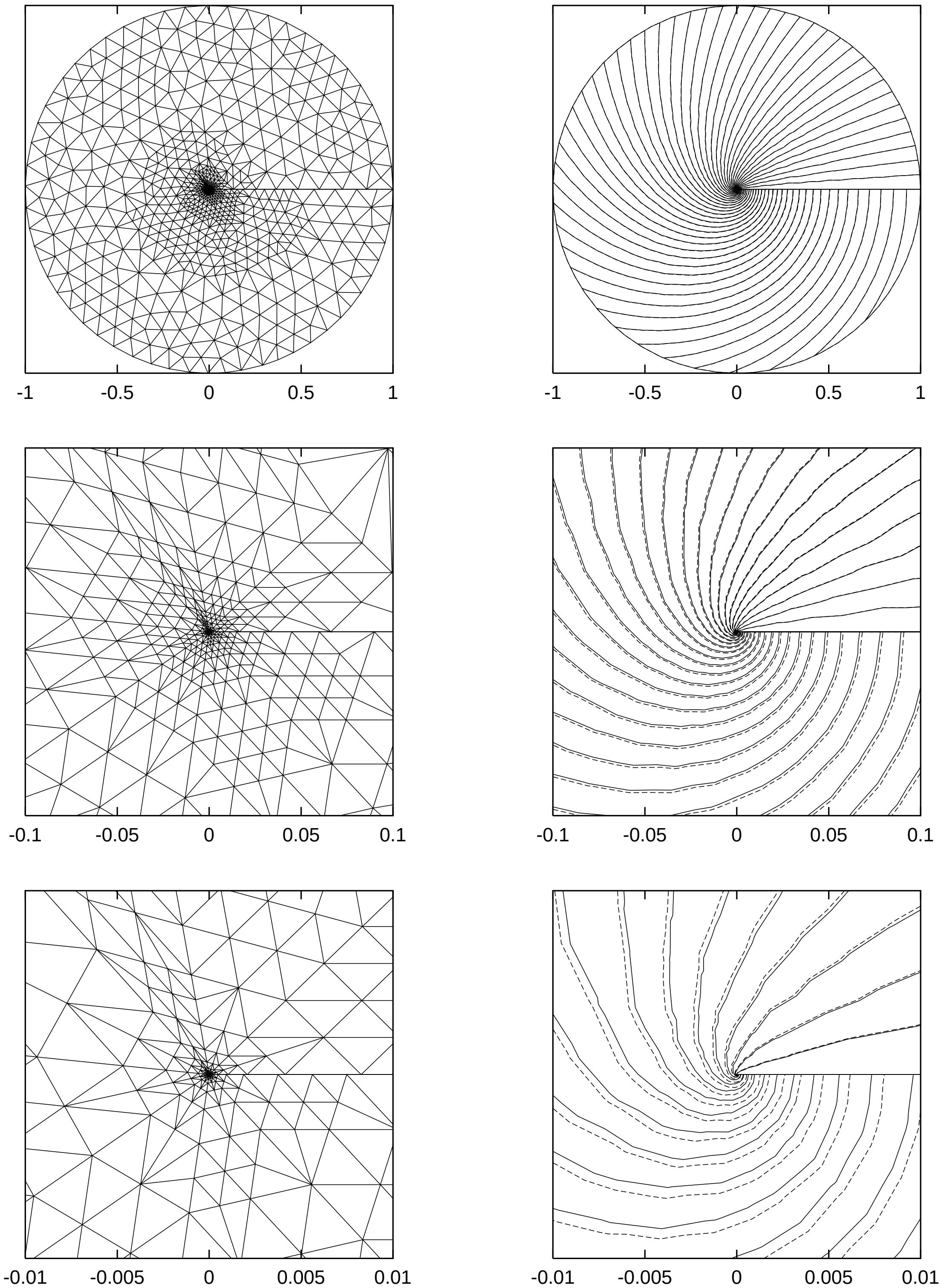

Figure 10: Singular diffusion problem, red-green refinement with $\eta = 2 \cdot 10^{-4}$ after 12 level of refinement ($nelem = 1602$) – mesh and isolines of u_h (full line) and $\Pi_h u$ (dashed line) with zooms.

numel	*nelem*	h	e_h	CPU (s)
125	127	0.1783	1.9281	7
500	546	0.0894	0.9905	9
2000	2314	0.0484	0.5340	29
8000	9332	0.0226	0.2655	252
32000	18950	0.0132	0.1346	87904

Table 4: Poisson problem with steep gradients – uniform meshes.

numel	ε_1	p	*nelem*	e_h	CPU (s)	
1	1E+10	100	361	0.18392	79	
1	1E+20	100	361	0.18392	79	
1	1E+30	100	361	0.18392	77	
1	1E+20	300	941	0.10783	152	
1	1E+10	300	945	0.10781	153	
1	1E+30	300	941	0.10783	146	
1	1E+10	600	1741	0.07753	287	
1	1E+20	600	1734	0.07666	295	
1	1E+30	600	1734	0.07666	301	Figure 11
1	1E+10	1000	2883	0.06475	593	
1	1E+20	1000	2908	0.06426	581	
1	1E+30	1000	2908	0.06426	586	

Table 5: Poisson problem with steep gradients – anisotropic meshes.

5.2.1 Uniform meshes

The same numerical method as in the previous section was applied. Table 4 contains the results of computation on four different uniform meshes. In contrast to the problem (69) – (70), the discretization error e_h of the problem (85) (given by (74)) differs from the minimal discretized error $e_h^{\min}$ (given by (76)) by the terms of order 10^{-4}. It is caused by the fact that the problem (85) has a smooth solution (86) and the used numerical scheme gives solution u_h almost identical with $\Pi_h u$. Therefore, Table 4 – Table 6 do not contain the values $e_h^{\min}$ and Figures 11 and 12 do not contain the isolines of $\Pi_h u$.

If we again suppose the relation (78) we determine the order of convergence as $\kappa = 1.007$ ($\beta = 11.19$), which corresponds to the theoretical results (72) ($\kappa = 1$ for regular problems).

5.2.2 Anisotropic meshes

Table 5 contains results of the solution of (85) on meshes achieved by AMA (all quantities have the same meaning as in Section 5.1.2).

Figure 11 shows an example of results from Table 5 - the triangulation and the corresponding contours of constant values of the numerical solution u_h are depicted here. The

η	No. of ref.	$nelem$	e_h	$e_h^{\min}$	CPU (s)	
1E-03	5	1041	0.3781	0.1906	35	
1E-04	6	2778	0.2343	0.1485	49	
1E-05	7	8583	0.1336	0.1225	175	Figure 12

Table 6: Poisson problem with steep gradients – red-green refinement.

expected grid alignment is easily viewed.

5.2.3 Isotropic mesh refinement

We again applied the red-green refinement method introduced in Section 5.1.3. In this case it is possible to apply the mesh refinement till the error indicator $g(T)$ is under the tolerance η for each triangle. The computation was performed for three values of the tolerance η. The results achieved are viewed in Table 6 and one of them is visualized in Figure 12.

5.3 Discussion of the results

From the results presented in Sections 5.1 and 5.2, we can conclude the following:

- The computations show that the discretization error e_h (74) is close to $e_h^{\min}$ (76) for both uniform and adapted meshes. This is given by the fact that the used numerical method (conforming linear finite element method) gives a sufficiently accurate solution for a given triangulation. This underlines the importance of the necessary condition (13).

- The global mesh refinement leads to an enormous requirement on the memory and CPU-time. It is absolutely impractical.

- To achieve the same level of the computational error, the grids adapted by AMA have a smaller number of elements than the grids adapted by the red-green refinement (RGR). Particularly for the second example the difference is remarkable.

- On the other hand, the CPU-time is higher for AMA than for RGR. It is caused by the simplicity of considered problem – scalar linear equation. Here the mesh adaption algorithm requires more time than the numerical solution of the Poisson equation. The top efficiency of AMA plays a role in practical problems, where the CPU-time remains the same for the mesh adaptation but it is much higher for the numerical solution of the considered problem.

- Observing results from Table 2 and Table 5, we see that whereas the increase of ε_1 does not cause essential improvement of results, the increase of p leads to the decrease of the computational error (and naturally to the increase of the number of elements). Therefore, we propose the following strategy to set suitable parameters $numel$, ε_1 and p:

    1. to prescribe $numel$ according to (68),

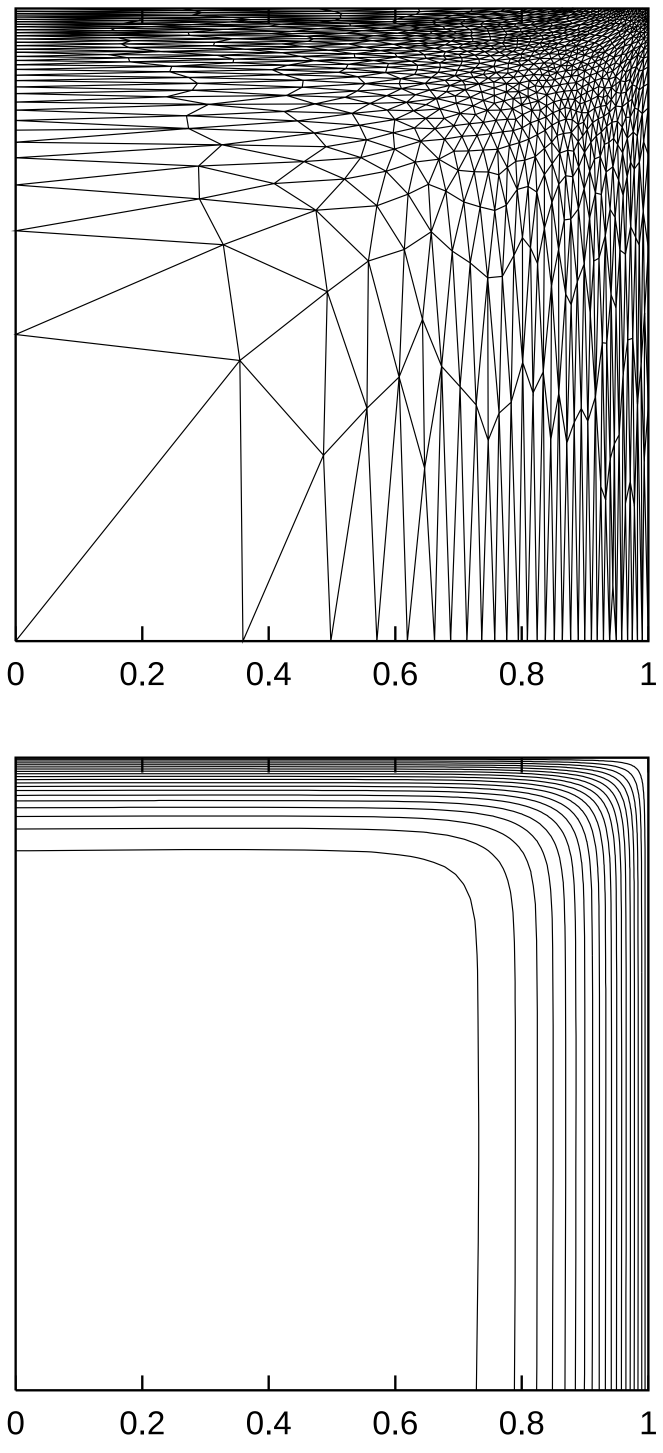

Figure 11: Poisson problem with steep gradients, anisotropic mesh adaptation with $numel = 1$, $\varepsilon_1 = 10^{30}$ and $p = 600$ ($nelem = 1734$) – mesh and isolines of u_h.

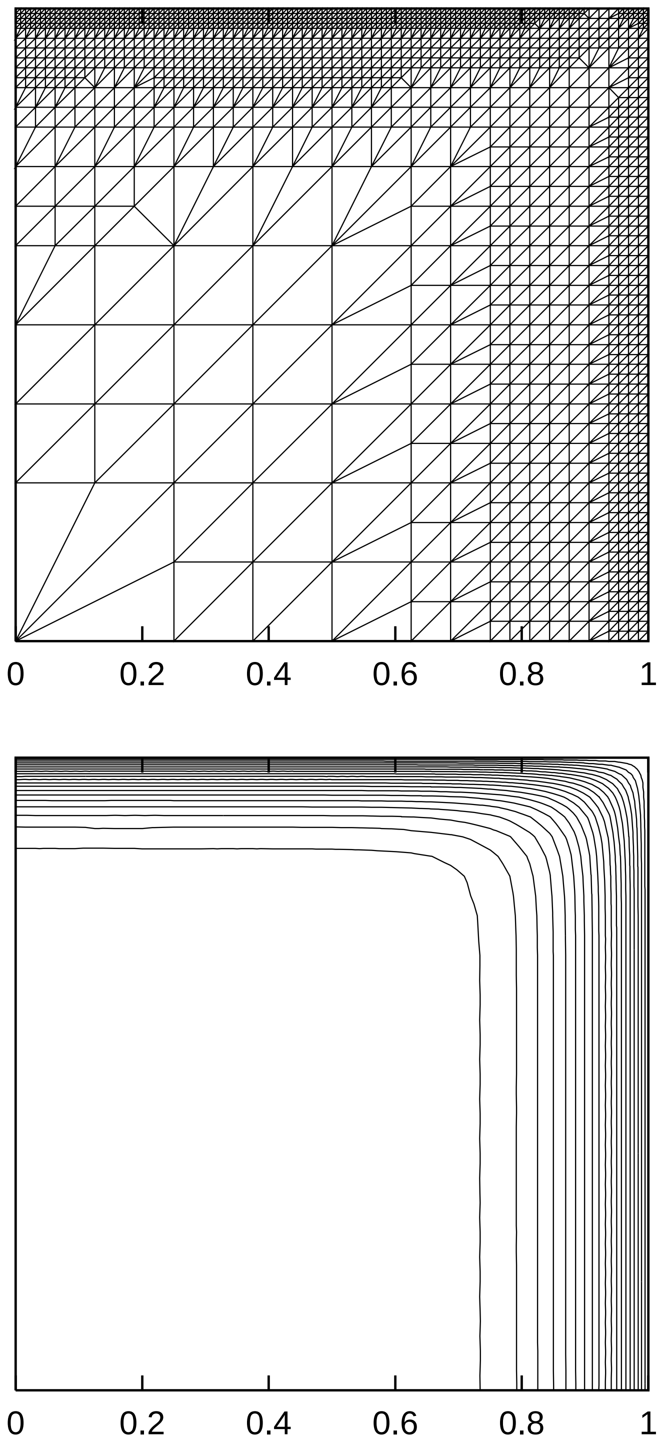

Figure 12: Poisson problem with steep gradients, red-green refinement with $\eta = 10^{-5}$ ($nelem = 8583$) – mesh and isolines of u_h.

2. to set ε_1 sufficiently high, e.g. 10^{20}, see (64),
3. to start with a small p and to increase successively its value till the number of elements is acceptable from the point of view of the computer memory and CPU time.

6 Application of AMA for transonic flow

We present results of computational fluid dynamics based on the AMA algorithm. We focus on the problem of transonic flow with strong discontinuities (shock waves) which require anisotropic meshes to achieve high quality results. We apply the AMA method to the solution of inviscid transonic flow around the NACA0012 profile with inlet Mach number $M_{\text{inlet}} = 2$ and angle of attack $\alpha = 0$.

In the space-time cylinder $Q_T = \Omega \times (0, T)$ we consider the first order hyperbolic system

$$\frac{\partial \boldsymbol{w}}{\partial t} + \sum_{s=1}^{2} \frac{\partial \boldsymbol{f}_s(\boldsymbol{w})}{\partial x_s} = 0 \tag{87}$$

describing inviscid compressible flow in a plane bounded domain Ω and time interval $(0, T)$. Here

$$\boldsymbol{w} = (\rho,\, \rho v_1,\, \rho v_2,\, e)^{\mathrm{T}}, \quad \boldsymbol{w} = \boldsymbol{w}(\boldsymbol{x}, t), \quad \boldsymbol{x} \in \Omega, \quad t \in (0, T),$$
$$\boldsymbol{f}_s(\boldsymbol{w}) = (\rho v_s,\, \rho v_s v_1 + \delta_{s1} p,\, \rho v_s v_2 + \delta_{s2} p,\, (e + p)\, v_s)^{\mathrm{T}}$$

and p is given by the state equation

$$p = (\gamma - 1)\,(e - \rho|\boldsymbol{v}|^2/2). \tag{88}$$

We use the standard notation: t – time, $\boldsymbol{x} = (x_1, x_2)$ – Cartesian coordinates, ρ – density, p – pressure, e – total energy, $\boldsymbol{v} = (v_1, v_2)$ – velocity, δ_{ij} – Kronecker delta, $\gamma > 1$ is the Poisson adiabatic constant. The initial condition and a set of boundary conditions complete the above system. For their description see, e.g., [17]. The system (87) – (88) is discretized by the cell-centred finite volume method on the triangular grid, see, e.g., [18], [20].

The piecewise linear approximate solution was updated using AMA technique. Eight levels of mesh adaptation were computed. We prescribed axial symmetry along $y = 0$ and we put $u := \rho$ (=density) in the computation of the Hesse matrixes $\boldsymbol{H}(P_i)$ given by (46).

The final mesh and the corresponding distribution of Mach number are plotted in Figure 13. The distribution of the pressure coefficient along the profile

$$c_p = -\frac{p - p_\infty}{\frac{1}{2}\rho_\infty |\boldsymbol{v}_\infty|^2} \tag{89}$$

is viewed in Figure 14. The variables p_∞, ρ_∞, and $|\boldsymbol{v}_\infty|$ are the values of the pressure, density, and magnitude of velocity of the inflow at infinity, respectively. The use of the AMA technique leads to the computation of sufficiently sharp shock waves.

This is a kind of a qualitative result. Very often, the engineers are interested in the distribution of flow quantities (pressure, Mach number etc.) along the profile. It could be important also in the computation of lift and drag coefficients. We refer at this point to results obtained with the described AMA technique even for viscous flow in [16].

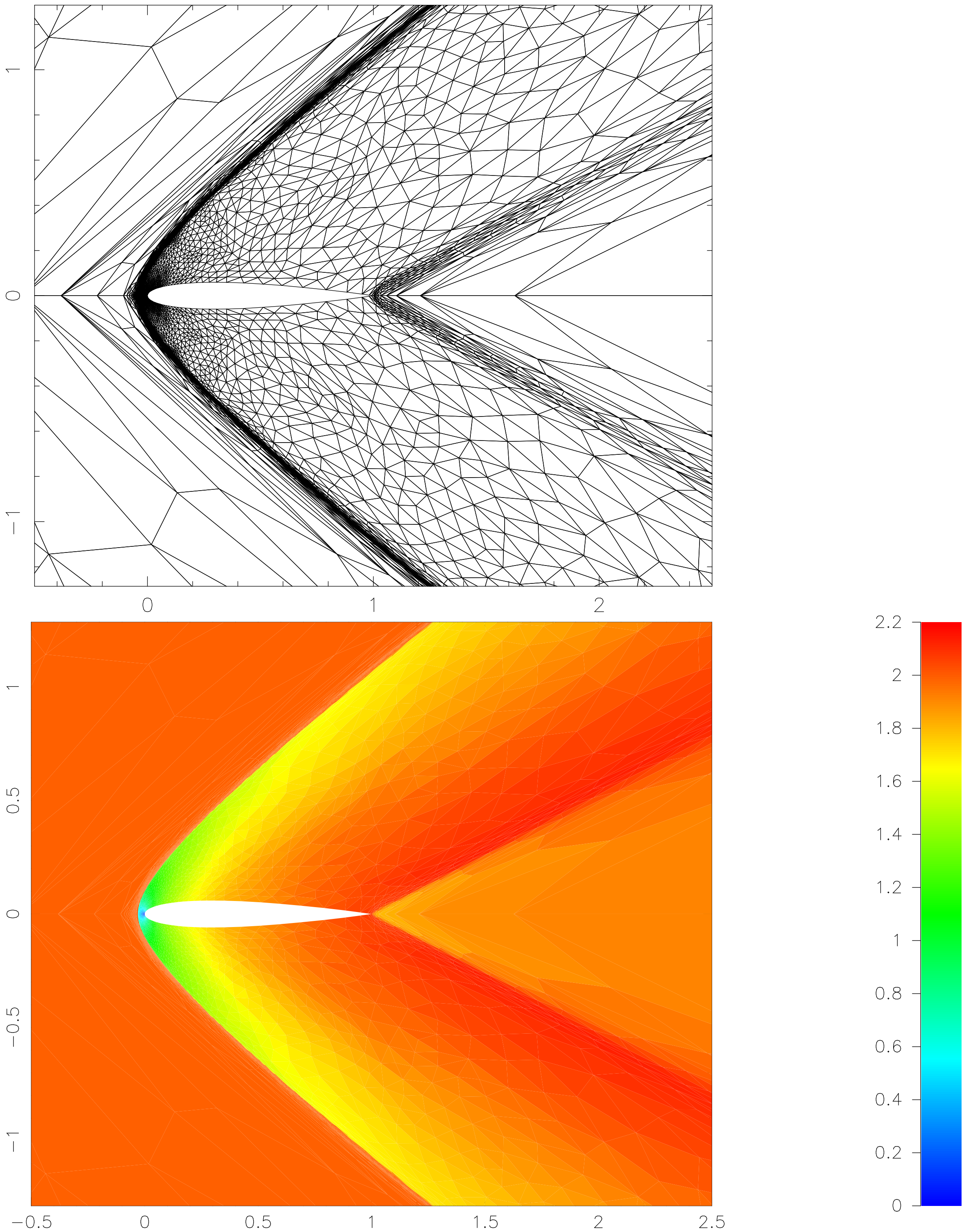

Figure 13: Inviscid flow around NACA0012 profile with $M_{\text{inlet}} = 2$, triangulation produced by AMA and the corresponding distribution of Mach number.

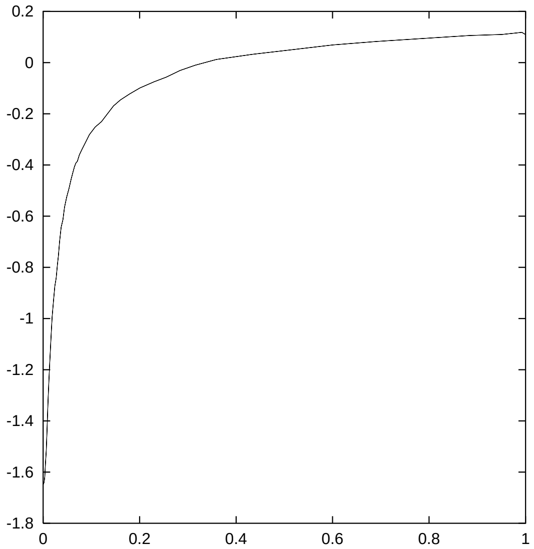

Figure 14: Inviscid flow around NACA0012 profile with $M_{\text{inlet}} = 2$, distribution of the pressure coefficient c_p along the profile.

7 Conclusion

We have developed an efficient mesh adaptation method for the numerical solution of an arbitrary boundary value problem on triangular grids. Both test examples confirm that the method presented can successfully resolve problems with singularities or steep gradients. To achieve a given error tolerance, AMA generates the grids with significantly lower number of triangles than the standard adaptive method. The application to challenging industrial problems gives satisfactory results. Moreover, we give a hint how to control the number of elements of a mesh (parameter *numel*), aspect ratio (parameter ε_1), and the transition of the coarsest part of the mesh to the finest one (parameter p).

The application of the AMA technique is not restricted only to CFD problems but it can be used also in other fields of computational science, e.g. the thermoregulation of premature infants [5].

References

[1] Ph. Angot, V. Dolejší, M. Feistauer, and J. Felcman. Analysis of a combined barycentric finite volume – nonconforming finite element method for nonlinear convection-diffusion problems. *Appl. Math.*, 43(4):263–310, 1998.

[2] T. Apel. *Anisotropic Finite Elements: Local Estimates and Applications.* Teubner, Stuttgart - Leipzig, 1999.

[3] T. Apel, S. Nicaise, and J. Schöberl. Finite element methods with anisotropic meshes near edges. In P. Neittaanmäki and M. Křížek, editors, *Finite Element Methods for Three-dimensional Problems*, volume 15 of *GAKUTO Internat. Series, Math. Sci. Appl.*, pages 1–8, Tokyo, 2001. University of Jyväskylä, GAKKOTOSHO CO., LTD.

[4] R. Bank, A. Sherman, and A. Weiser. Refinement algorithm and data structures for regular local mesh refinement. In R. Stepleman et al., editor, *Scientific Computing*, volume 44, pages 3–17. IMACS North–Holland, Amsterdam, 1983.

[5] M. Breuss, V. Dolejší, and A. Meister. On an adaptive method for heat conduction problems with boundary layers. *Preprint Hamburger Beiträge zur Angenwandten Mathematik.* (submitted to Computing and Visualization in Science).

[6] G. C. Buscaglia and E. A. Dari. Anisotropic mesh optimization and its application in adaptivity. *International Journal for Numerical Methods in Engineering*, 40:4119–4136, 1977.

[7] M. J. Castro-Díaz, H. Borouchaki, P. L. George, F. Hecht, and B. Mohammadi. Anisotropic Adaptive Mesch Generation in Two Dimensions for CFD. In J.-A. Désidéri, C. Hirsch, P. Le Tallec, M. Pandolfi, and J. Périaux, editors, *Computational Fluid Dynamics '96*, pages 181–186, Paris, 1996. Wiley, Chichester.

[8] P. G. Ciarlet. *The Finite Elements Method for Elliptic Problems.* North-Holland, Amsterdam, New York, Oxford, 1979.

[9] B. Cockburn. An introduction to the discontinuous Galerkin method for convection-dominated problems.

[10] E. F. D'Azevedo and R. B. Simpson. On optimal interpolation triangle incidences. *SIAM. J. Sci. Statist. Comput.*, 10:1063–1075, 1989.

[11] E. F. D'Azevedo and R. B. Simpson. On optimal triangular meshes for minimizing the gradient error. *Numer. Math.*, 59:321–348, 1991.

[12] V. Dolejší. Numerical Solver for Compressible Flows – Anisotropic Mesh Adaption. In K. Kozel M. Feistauer, R. Rannacher, editor, *Numerical Modelling in Continuum Mechanics*, pages 246–253. Matfyzpress, Praha, 1997.

[13] V. Dolejší. Adaptive methods for the numerical solution of the compressible Navier–Stokes equations. In K. D. Papailiou, D. Tsahalis, J. Périaux, C. Hirsch, and M. Pandolfi, editors, *Computational Fluid Dynamics'98*, volume 1, pages 393–397. ECCOMAS, John Wiley & Sons, 1998.

[14] V. Dolejší. Anisotropic mesh adaptation for finite volume and finite element methods on triangular meshes. *Computing and Visualization in Science*, 1(3):165–178, 1998.

[15] V. Dolejší and Ph. Angot. Finite Volume Methods on Unstructured Meshes for Compressible Flows. In F. Benkhaldoun and R. Vilsmeier, editors, *Finite Volumes for Complex Applications (Problems and Perspectives)*, pages 667–674. Hermes, Rouen, 1996.

[16] V. Dolejší, M. Feistauer, and J. Felcman. Flow computations using combined finite volume–finite element method. Preprint, Charles University, Prague, 2001.

[17] M. Feistauer. *Mathematical Methods in Fluid Dynamics.* Longman Scientific & Technical, Harlow, 1993.

[18] J. Felcman and V. Dolejší. Adaptive Methods for the Solution of the Euler Equations in Elements of the Blade Machines. *ZAMM*, 76(S4):301–304, 1996.

[19] J. Felcman and V. Dolejší. Investigation of accuracy for higher order finite volume schemes. *Engineering Mechanics*, 5(5):327–337, 1998.

[20] J. Felcman, V. Dolejší, and M. Feistauer. Adaptive Finite Volume Method for the Numerical Solution of the Compressible Euler Equations. In J. Périaux S. Wagner, E. H. Hirschel and R. Piva, editors, *Computational Fluid Dynamics '94*, pages 894–901. John Wiley and Sons, Stuttgart, 1994.

[21] M. Fortin, M.-G. Vallet, J. Dompierre, Y. Bourgault, and W. G. Habashi. Anisotropic Mesh Adaptation: Theory, Validation and Applications. In J.-A. Désidéri, C. Hirsch, P. Le Tallec, M. Pandolfi, and J. Périaux, editors, *Computational Fluid Dynamics '96*, pages 174–180, Paris, 1996. Wiley, Chichester.

[22] W. G. Habashi, M. Fortin, D. Ait ali Yahia, S. Boivin, Y.Bourgault, J. Dompierre, M. P. Robichaud, A. Tam, and M. G. Vallet. Anisotropic mesh optimization: Towards a solver-independent and mesh-independent CFD. In *Compressible Fluid Dynamics*, VKI Lecture Series 1996-06. von Karman Institute for Fluid Dynamics - Concordia University, August 1996.

[23] D. Kröner. *Numerical Schemes for Conservation Laws.* Wiley Teubner, Stuttgart, 1997.

[24] D. Kröner and M. Rokyta. Convergence of upwind finite volume schemes for scalar conservation laws in 2D. *SIAM J. Numer. Anal.*, 31:324–343, 1994.

[25] R. B. Simpson. Anisotropic mesh transformations and optimal error control. *Applied Numer. Math.*, 14:183–198, 1994.

[26] R. Temam. *Navier–Stokes Equations. Theory and numerical analysis.* North–Holland, Amsterdam–New York–Oxford, 1977.